ATTACHMENT 3
U.S. Department of Energy
FEDERAL ASSISTANCE REPORTING CHECKLIST
AND INSTRUCTIONS

1. Identification Number: DE-FE0004566	2. Program/Project Title: "Prototyping and testing a new volumetric curvature tool for modeling reservoir compartments and leakage pathways in the Arbuckle saline aquifer: Reducing uncertainty in CO2 storage and permanence"			
3. Recipient: University of Kansas				
4. Reporting Requirements:	Frequency	No. of Copies		Addresses

4. Reporting Requirements:	Frequency	No. of Copies	Addresses
A. MANAGEMENT REPORTING ☒ Progress Report ☒ Special Status Report	Q A	Electronic Version to NETL>	*FITS@NETL.DOE.GOV*
B. SCIENTIFIC/TECHNICAL REPORTING * (Reports/Products must be submitted with appropriate DOE F 241. The 241 forms are available at https://www.osti.gov/elink)			
Report/Product Form ☒ Final Scientific/Technical Report DOE F 241.3 ☒ Conference papers/proceedings/etc.* DOE F 241.3 ☐ Software/Manual DOE F 241.4 ☒ Other (see special instructions) Topical DOE F 241.3 * *Scientific/technical conferences only*	FG A A	Electronic Version to E-link>	*http://www.osti.gov/elink-2413* *http://www.osti.gov/elink-2413* *http://www.osti.gov/estsc/241-4pre.jsp*
C. FINANCIAL REPORTING ☒ SF-425, Federal Financial Report	Q, FG	Electronic Version To NETL>	*FITS@NETL.DOE.GOV*
D. CLOSEOUT REPORTING ☒ Patent Certification ☒ Property Certificate ☐ Other	FC FC	Electronic Version To NETL>	*FITS@NETL.DOE.GOV*
E. OTHER REPORTING ☒ Annual Indirect Cost Proposal ☒ Annual Inventory Report of Federally Owned Property, if any ☐ Other	A A	Electronic Version To NETL>	*FITS@NETL.DOE.GOV*
F. AMERICAN RECOVERY AND REINVESTMENT ACT REPORTING ☐ Reporting and Registration Requirements			*http://www.federalreporting.gov*

FREQUENCY CODES AND DUE DATES:
   A - As required; see attached text for applicability.
   FG - Final; within ninety (90) calendar days after the project period ends.
   FC - Final - End of Effort.
   Q - Quarterly; within thirty (30) calendar days after end of the calendar quarter or portion thereof.
   S - Semiannually; within thirty (30) calendar days after end of project year and project half-year.
   YF - Yearly; 90 calendar days after the end of project year.
   YP - Yearly Property - due 15 days after period ending 9/30.

5. SPECIAL INSTRUCTIONS:
   • The forms identified in the checklist are available at <u>DOE Financial Assistance Forms Page</u>. Alternate formats are acceptable provided the contents remain consistent with the form.
   • See Federal Assistance Reporting Instructions on the following page.

QUARTERLY PROGRESS REPORT

Award Number: DE-FE0004566

Recipient

University of Kansas Center for Research and
The Kansas Geological Survey
1930 Constant Avenue
Lawrence, Kansas 66047

Title

"Prototyping and testing a new volumetric curvature tool for modeling
reservoir compartments and leakage pathways in the Arbuckle saline aquifer: reducing
uncertainty in CO$_2$ storage and permanence"

Project Director/Principal Investigator: Jason Rush
Joint Principal Investigators: Jason Rush/Lynn Watney

9th Quarter Progress Report

Date of Report: 2/22/2013

Authors: Jason Rush and W. Lynn Watney

Period Covered by this Report: October 1, 2012 December 31, 2012

Executive Summary

The contract for the project, "*Prototyping and testing a new volumetric curvature tool for modeling reservoir compartments and leakage pathways in the Arbuckle saline aquifer: reducing uncertainty in CO_2 storage and permanence*," was signed with U.S. DOE on October 1, 2010. The project is collaboration between the Kansas Geological Survey (KGS) and its industry partner MVP LLC (a partnership between Murfin Drilling Company and Vess Oil Corporation). The project study area is located in Ellis County, Kansas.

Accomplishments this quarter include: (1) ASME project peer review; (2) completed facies and structural interpretation of McCord-A 20H image log; (3) classified facies and constructed facies probability maps; (4) completed construction of final facies logs and facies model; (5) constructed final fault model; (6) constructed final porosity model; and (7) constructed permeability model.

Stratigraphic, sedimentologic, and structural analysis of the image log was completed. Five facies were identified using image and lithology logs. These facies are similar to those described from the L. Hadley-4 core. Unexpectedly, breccia fabrics are present throughout the well bore and were not limited to the paleokarst system as imaged by seismic volumetric curvature (VC). Observations from the McCord-A 20H image log, L. Hadley-4 core, and the KGS 1-32 core provide important new clues to the depositional and post-depositional history of the Arbuckle. Evidence from the wells indicates that the Arbuckle was deposited in a restricted peritidal to supratidal setting. Bedding and strata-bound breccias are thought to record evaporite karst. This type of strata is preserved outside VC-imaged dolines and solution-modified fractures and faults. If true, this style of stratigraphic architecture will have important implications for simulation-based studies of the Arbuckle.

Faults and fractures identified from the image log have been tied to a new fault model consisting of 201 independent faults and dilational fractures. Facies probability maps were generated from the VC map and used as a secondary variable during sequential indicator simulation. The new facies model was used to bias the porosity and permeability logs during well-specific upscaling. All 3-D static property models were conditioned to the 3-D facies model. Co-rendering of the various depth-converted seismic attributes and geocellular fault, facies, and property models provide a compelling case for careful integration of data and the predictive quality of VC. Well head samples have been collected from four well for geochemical analyses. Other than subtasks related to XRD and geochemical studies, all milestones (1.1–2.3) have been completed.

DISCUSSION
Approach:

Image log analysis—Image interpretation consisted of describing 1) structural features and 2) facies. Four types of structural features are identifiable from the image log (Fig. 1). These consist of conductive fractures/faults, partially conductive faults/fractures, faults (having obvious offset), and bedding planes. Sand and clay are present within faults and dilational fractures. Fractures occur more frequently near and within the VC-identified, fault-bound doline (Fig. 2). Fault and fracture picks have been tied to their respective fault. Breccias were anticipated only in the uppermost Arbuckle and within the paleocavern. However, breccias were unexpectedly found along the entire length of the image log. Bedding indicators are dominantly recorded outside of the paleocavern (Fig. 3). The lithology logs indicate a fair amount of siliciclastics and clays in the upper Arbuckle and within the paleocavern. Non-touching vugs are only present outside the paleocavern.

Louck's (1999) paleokarst classification system was used for describing facies (Fig. 4). Five types of facies were described using a combination of the image log and lithology logs. These include: 1) crackle breccia, 2) chaotic breccia, 3) matrix-supported breccia, 4) dolostone beds, and 5) dilational fractures. Matrix-supported breccias coincide with high silica measurements. Image examples of both structural- and facies-based interpretations are provided in Figures 5–14.

Fault modeling—
The final fault model has been constructed. Faults in the latest model correspond to high negative volumetric curvature values (Fig. 15). The fault model was constructed using vertical pillars, which is consistent with fault geometries revealed by the PSDM volume. Faults intersecting the McCord-A 20H well bore are tied to their corresponding image log pick. This model contains 201 faults, which were successfully gridded using Rock Deformation Research's (RDR) Petrel module. The RDR module builds a grid by individually rotating each fault to a "best fit" plane. The 3-D structural grid contains 2,021,250 cells (x=275; y=98; x=75). The average cell dimension is: x=44.6 ft, y=75.2 ft, and z=9.8 ft. All property models are assigned the same 3-D grid geometry.

Additional faults can be observed in the 3-D seismic volume (Fig. 16). However, their inclusion is not practical because: (1) individual 3-D grid cells cannot accommodate more than one fault pillar, and (2) the project objective is to evaluate seismic VC, which is of lower resolution than the 3-D seismic volume.

Facies modeling—Five facies were described using the L. Hadley-4 core and McCord-A 20H lithology and image logs (Fig. 1). A facies log was constructed using a sample spacing of 0.5 ft. The L. Hadley-4 well is located outside the study area (Fig. 17). In order to use core descriptions of facies and routine core measurements from the L. Hadley-4 well, its logs (i.e., GR, XPHI) were compared to wells within the study area, so that it could be used as a "pseudo well." The best match is to Colahan-B29. The surface location for the L. Hadley-4 pseudo well is immediately NE of Colahan-B29. The KB elevation for the pseudo well was changed so that the Arbuckle log pick intersected the Arbuckle surface. The facies logs were upscaled using the "most of" averaging method.

Well log-based facies distributions are biased in several ways. First, the McCord-A 20-H, prior to its landing (3618–4309-ft MD), was drilled outside the margins of the doline and passed vertically through the stratigraphic section. A facies log from this part of the test boring would be biased toward "unaffected" host strata. Then the test boring passes horizontally through the paleocavern system (4309–5351-ft MD). Here, the facies log is biased toward mechanically compacted rock fabrics, such as crackle and chaotic breccias. The final segment, drilled horizontally through unaffected host strata, is biased strongly toward bedded dolostones. The Hadley-4 core provides additional constraint on facies distributions for the uppermost Arbuckle. An additional complication arises because no modern wireline logs exist for the few basement penetrations in the area. Owing to these uncertainties, the facies distributions input into the 3-D modeling algorithm were strongly biased toward VC-derived facies probability maps (Fig 18). The result is a more geologically realistic facies model (Fig 19).

Three probability maps were constructed to constrain the spatial distribution of the facies model. Their distribution is based on outcrop analog studies of paleokarst. The volumetric curvature map was used to delineate three main facies associations: (1) those coincident with VC-imaged fractures and faults (facies: dilational fracture fill); (2) those coincident with dolines (facies: chaotic and crackle breccia); and (3) those coincident with host strata (facies: bedded dolostone and matrix-supported breccia). It should be reiterated that strata-bound breccias probably formed in response to evaporite dissolution and burial compaction. These strata-bound, comparatively thin-bedded breccias (meter-scale) reflect an arid, peritidal to supratidal setting in contrast to seismic-scale paleocaverns linked to glacio-eustatic, vadose karst processes.

The facies were modeled using sequential indicator simulation and deterministically derived 2-D facies trends. Using this method, at each grid cell the algorithm: (1) searches for nearby data, (2) builds an uncertainty distribution using indicator Kriging, and (3) then selects a simulated value from the uncertainty distribution. Kriging equations are modified locally to account for azimuthal changes in facies continuity. Facies variogram calculations are problematic because facies continuity is nested within/or outside of paleokarst features and, therefore, facies patterns exhibit a locally varying azimuth. As such, the lateral range of each variogram reflects their individual, average lateral continuity across the field (fracture fill xy: 50 ft; bedded dolomite and matrix supported breccia xy: 1000 ft; crackle and chaotic breccia xy: 500 ft). The vertical variogram ranges are a function of karst penetration and fracture depth (fracture fill: 100 ft; paleocavern fill: 20 ft; host strata: 5–15 ft). The nugget for all facies was set artificially low (0.01) because outcrop studies indicate that the nugget is largely a function of sufficiently small-scale heterogeneities (<1 ft) that do not impact effective reservoir properties.

Porosity modeling—In contrast to well data, seismic data is areally extensive over the reservoir and is, therefore, of great value in constraining facies and porosity trends within models. A PSTM acoustic impedance inversion solution was generated. However, because it is in time, it offers little 3-D utility other than visualization. Petrel's™ volume attribute processing (i.e., genetic inversion) was used to derive a PSDM porosity attribute to condition the revised porosity model. A new seismic volume was created by re-sampling (using the original exact amplitude values) the PSDM 50-ft above the Arbuckle and 500-ft below (i.e., approximate basement). A cropped PSDM volume

and porosity logs (XPHI) were used as learning inputs during neural network processing. A correlation threshold of 0.85 was selected and 10,000 iterations were run to provide the best correlation. The resulting porosity attribute was then re-sampled, or upscaled (i.e., average method), into their corresponding 3-D property grid cell (Fig. 20).

The latest porosity model was constructed using sequential Gaussian simulation (SGS) (Fig. 21). The porosity logs were biased to the 3-D facies model during arithmetic average upscaling. A normal porosity distribution was used as input for each facies during SGS. The same variogram settings used during facies modeling were also used during SGS of porosity. During SGS, the seismic porosity grid was used as a secondary variable for collocated co-Kriging and the correlation coefficient was arbitrarily set to 0.8 for each facies.

Permeability modeling—Fifty-five permeability measurements from L. Hadley-4 core plugs were upscaled using harmonic mean and bias to facies (Fig. 17). Core permeability values measured 0.001–4609.800 mD. Ranges per individual facies are as follows: fracture fill (0.01–e1.00 mD); bedded dolostones (0.31–16.29 mD); matrix-supported breccias (0.44–2059.57 mD); crackle breccia (0.01-4609.80 mD); chaotic breccia (0.01–e2000 mD). Permeability was modeled using SGS. A log normal permeability distribution was chosen for each facies because the sample size per facies is not statistically valid. Variogram ranges were set to the same range as facies. Probability maps were used as a local varying azimuth for their respective facies. Except for fracture fill, each facies was conditioned to the 3-D porosity model using collocated co-Kriging and a 0.8 correlation coefficient. The resulting permeability model reveals geologic complexity consistent with paleokarst analogs where the permeability architecture is dominantly strataform within host rock (Loucks, 1999: Fig. 22).

RESULTS

The RDR fault modeling module permitted gridding of complex fault geometries that are consistent with the VC interpretation. Such complex 3-D grid geometries are critical for assessing the utility of seismic VC using simulation techniques. If the structural grids are a crude approximation of the actual fault geometry, then all subsequent simulation scenarios will abide by the idiom *garbage in, garbage out*. The new structural provides a skeleton upon which to (1) construct fault/fracture damage zones using discrete fracture network (DFN) models and (2) generate local grid refinements to accommodate properties related to complex permeability patterns (e.g., clay smears, cataclastites). This new structural framework provides more than 50 fault-bound segments that will enhance compartmentalization studies (Fig. 23). The new facies probability maps and facies model provide a geologically realistic approximation of the stratigraphic architecture with collapsed paleocaves, suprastratal deformation, and strataform host rock (Fig. 24 A–B). Arbuckle geomorphology at the study area suggests capture via karst depressions and solution-enlargement of antecedent faults/fractures recorded by clastic-filled fissures (Fig. 24 C). Likewise, the facies used for the model are consistent to those observed in outcrop analog studies (Loucks 1999, Loucks et al. 2004) and subsurface studies of Ordovician paleokarst (Kerans, 1988). Effective porosity permeability, and flux across fault boundaries will be assessed during future simulation studies.

CONCLUSIONS:

Efforts for the next quarter will concentrate on DFN modeling, responding to the ASME peer review, and completing the continuation application for BP3. Additionally, well logs from the study area will be screened to determine if they have the requisite logs for processing additional lithology logs. These could be used to provide additional well control for facies modeling. An important revelation resulting from this project is the likely occurrence of evaporite karst. This has important implications for CCS characterization projects of Arbuckle strata in Kansas. Fluid behavior within reservoirs impacted by evaporite karst processes would have significantly better conformance than those overprinted by deeply penetrative vadose karst processes. It is also important to note that karst morphologies identified using VC attributes at Bemis-Shutts Field have not been observed at Wellington Field, Kansas. Determination of the drivers for this style of vadose paleokarst has important implications for CCS in Kansas. Constraining the age of exposure and the roll of accommodation is important for understanding and predicting the style of paleokarst and its impact on reservoir architecture.

One issue that should be addressed is the influence of the Arbuckle velocity model on intra-Arbuckle karst morphologies. The existing velocity model encompasses the interval from surface to top Arbuckle. As such reflectors below the Arbuckle/Simpson contact largely mimics the overlying Arbuckle surface. A PSDM volume that includes velocity profiles down to the basement would lead to a better understanding of karst morphologies and whether dilational fractures (i.e., fissures) and solution-enlarged faults are rooted in underlying basement structures.

Cost Status

Please refer to Attachment 1

Schedule/Milestone Status

Please refer to Attachment 2

BP1 Milestone Status: A three-month, no cost extension was granted to the project for BP1. Seismic reprocessing—including volume merging—was delayed because of protracted contract negotiations with numerous stakeholders. Signed agreements were finally in place by February 2011, some four months after award. The project is largely on schedule. BP1–BP2 milestone status is as follows:
  - Milestone 1.1 (completed): obtain field data including 3-D seismic, gravity magnetic, satellite imagery, production records, and well logs
  - Milestone 1.2 (completed): seismic processing and interpretation, VC-analysis, surface mapping, generate pre-spud geocellular model
  - Milestone 1.3 (completed): history match well performance using pre-spud

geocellular model

- Milestone 1.4 (completed): locate, permit, drill, and log horizontal borehole (i.e., McCord-A 20H)
- Milestone 2.1 (in progress): complete formation evaluation: log analysis, XRD, core analysis, and water geochemistry
- Milestone 2.2 (completed): complete final VC-attribute and seismic inversion

Changes in Approach or Aims

There have been no changes in approach or aims since the last quarterly report (8th).

Actual or Anticipated Problems

There are no updates regarding *actual or anticipated problems* since the last quarterly report (8th).

No problems that would jeopardize the project objectives have been encountered. Modifications to the SOPO are discussed above. Potential problems after the successful completion and logging of the horizontal test boring are not anticipated. A no-cost extension for BP1 was granted in early July. The presence of breccias and large faults as recorded by the full-bore micro-imager indicates the lateral has fulfilled the project objectives.

Absence or Key Personnel Changes

There are no updates regarding *absence or key personnel changes* since the last quarterly report (8th).

Saibal Bhattacharya, previous Joint PI, resigned from the KGS in May 2011. Lynn Watney has agreed to assume Joint-PI responsibilities and assist with managerial tasks. A search is underway for a permanent simulation engineer. Gene Williams, a consultant, the principal in Williams Petroleum Consulting in Houston, was contracted to build the series of simulations required for the project. He has considerable experience with CO_2-EOR comes highly recommended by staff at CMG. Mr. Williams comes with the expertise and experience that is needed to fit into the project and no disrupt the workflow. Eugene Holubynak joined the KGS ERS in 2012 as a simulation engineer. He will be conducting additional simulation-based investigations.

All other key personnel, as listed in the proposal, continue to work for and are part of this study. No personnel changes are anticipated at this point in time. KGS has also hired undergraduate engineer, Aadish Gupta, whose primary is to coordinate handling of well data and building input data files for geomodels and simulation. Also, Mina Fazelalavi, a graduate engineer from KU to conduct quality control, normalization, and analysis of LAS wireline log files for the DOE projects and to assist in building integrated geomodels suited for simulation.

Technology Transfer

Results to date were presented in October 2012 to the ASME Peer Review board in Pittsburgh. The project website (http://www.kgs.ku.edu/PRS/Bemis/index.html) has been constructed and is available for public access. The project web site will display all results and interpretations obtained from this study and will be maintained by the KGS. Technology transfer activities are anticipated to begin during the final half of the last year, when all data collection has been completed, and analysis, interpretation, and modeling are in progress to demonstrate and validate the feasibility of using volumetric curvature analysis to characterize paleokarst reservoir compartmentalization to better model of CO_2 storage and permanence in saline aquifers such as the Arbuckle in Kansas.
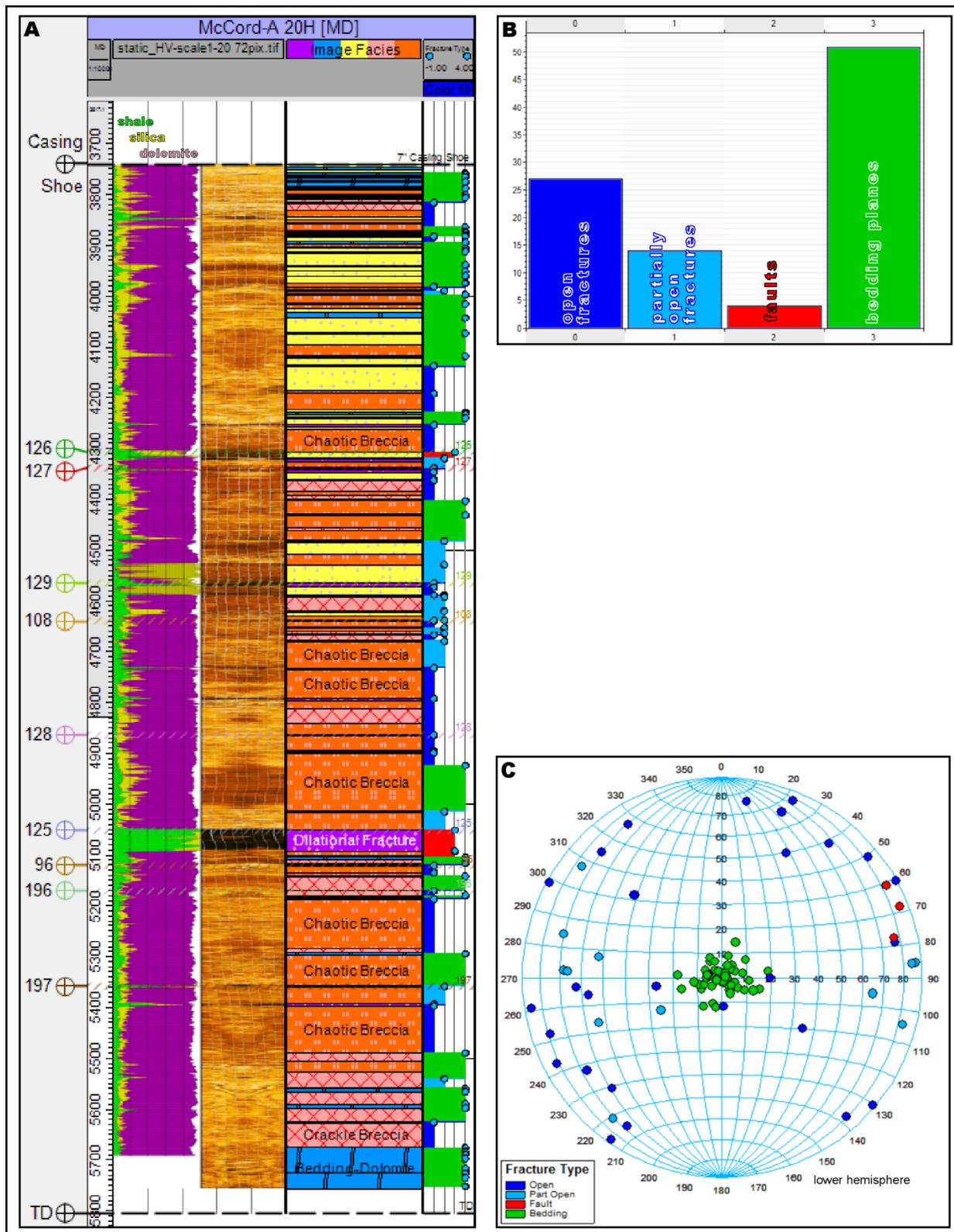
Figure 1. **A)** Lithology log, static image log, facies, and structural interpretation. **B)** Histogram showing distribution of open fractures (0), partially open fractures (1), faults (2), and bedding planes (3). **C)** Schmidt stereonet of fracture, fault, bedding orientations.
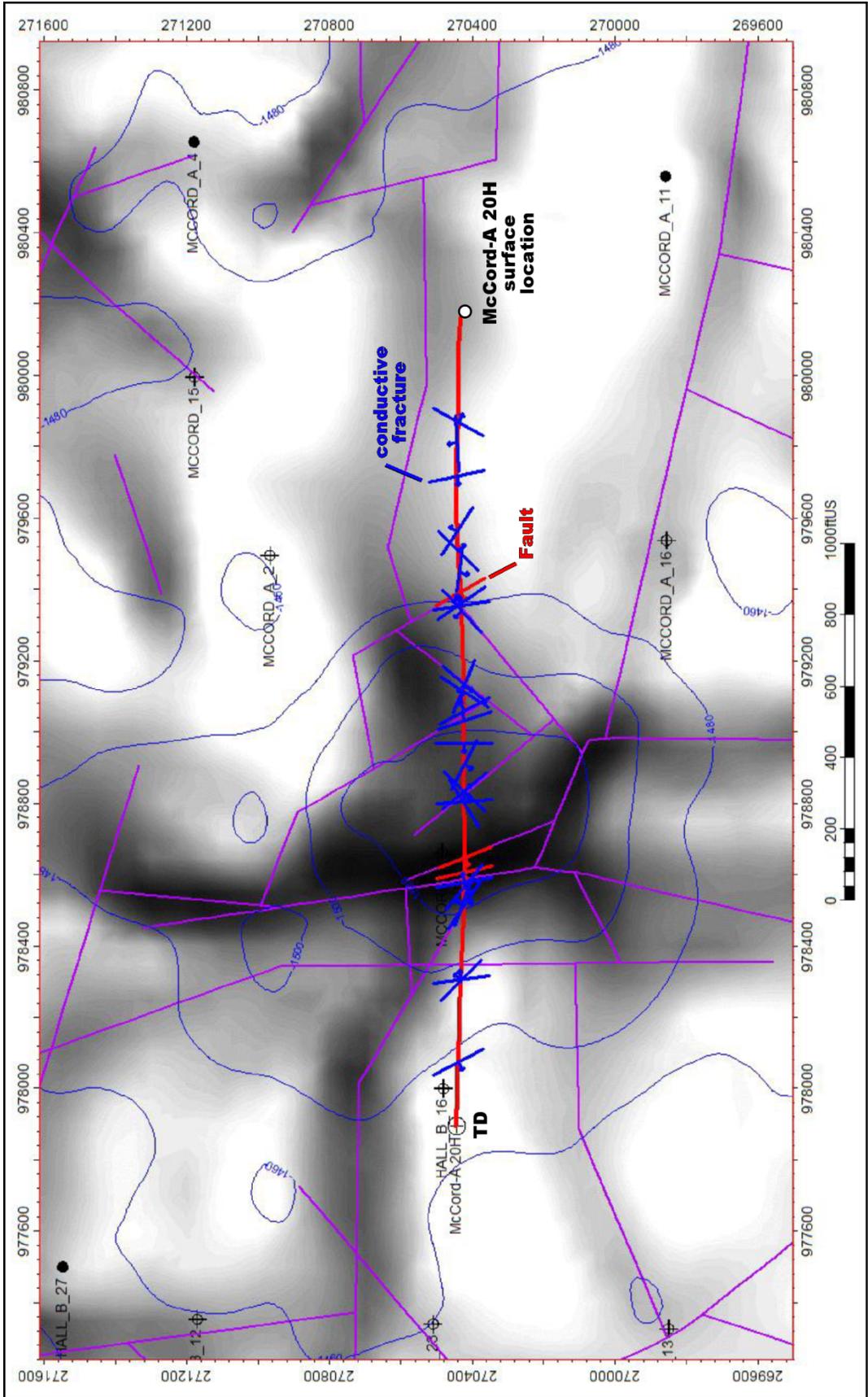
Figure 2. Map showing large fault/fractures corresponding to negative attributes from seismic volumetric curvature (VC). Posted along the McCord-A 20H well path are the strike of high-angle fault and fractures identified from interpretation of bore hole image logs. Faults and fractures identified from VC have been correlated to image log picks at the same orientation. Some picks can not be included as faults or fractures within the fault model because their spacing is smaller than the grid size.

9
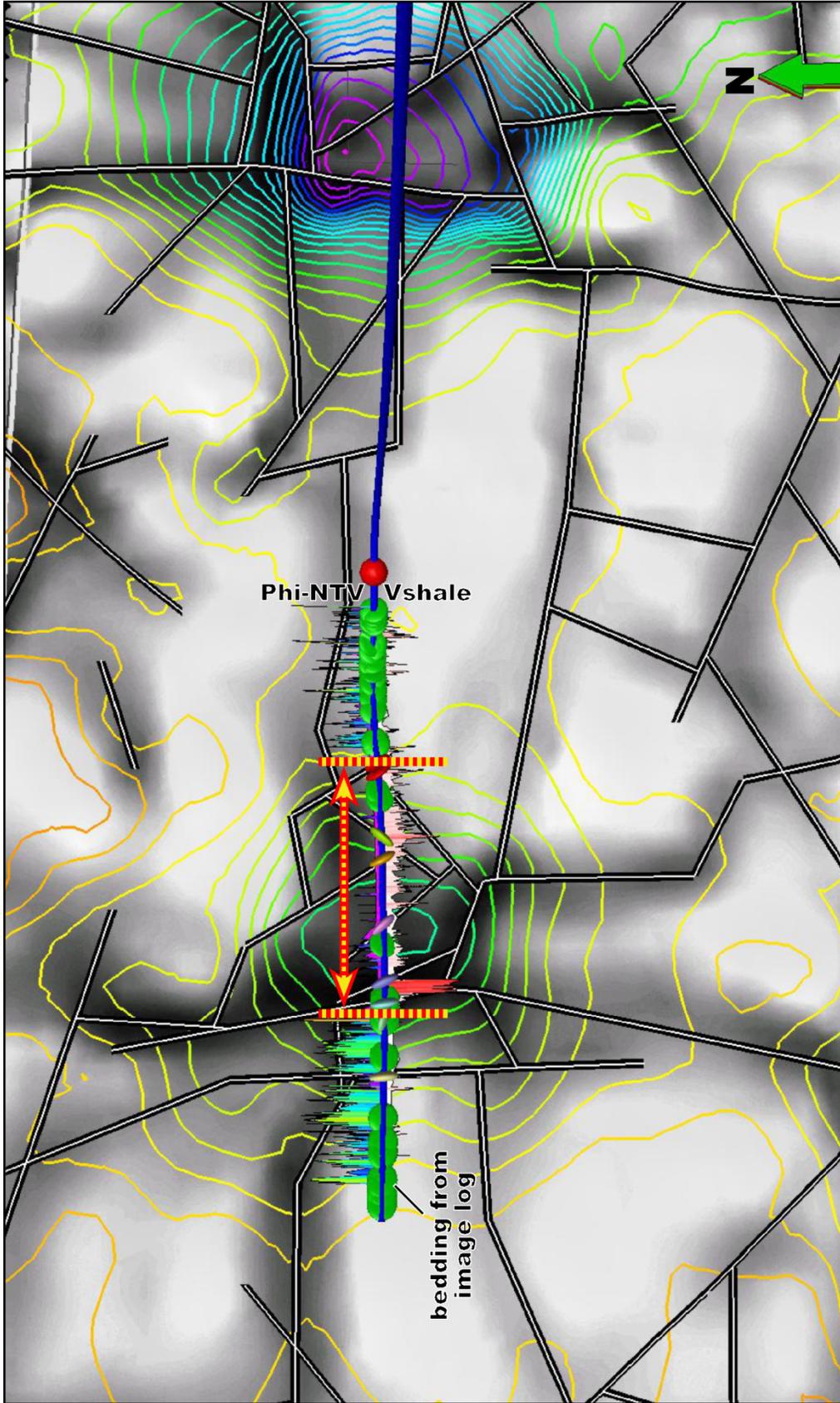
Figure 3. Map, well track, and logs showing evidence of compartmentalization consistent with VC-guided fault interpretation. Area between red and yellow dashed lines indicates changes in lithology and pore types within collapsed paleocavern. The log track Phi-NTV indicates the percent of non-touching vugs. Non-touching vugs were likely destroyed during collapse and brecciation processes and further modified by diagenetic processes related to enhanced fracture permeability. The shale volume log indicates a greater occurrence of silica throughout the paleocavern and lesser amount in the uphole Arbuckle section. This is consistent with the presence of interbedded sands in the upper Arbuckle and overlying Simpson. Dilational fractures would have functioned as conduits that introduced siliciclastics into the open paleocavern. Additionally, vadose diagenetic processes would have generated insoluble residues that were preferentially deposited within dilational fractures and passageways.

10
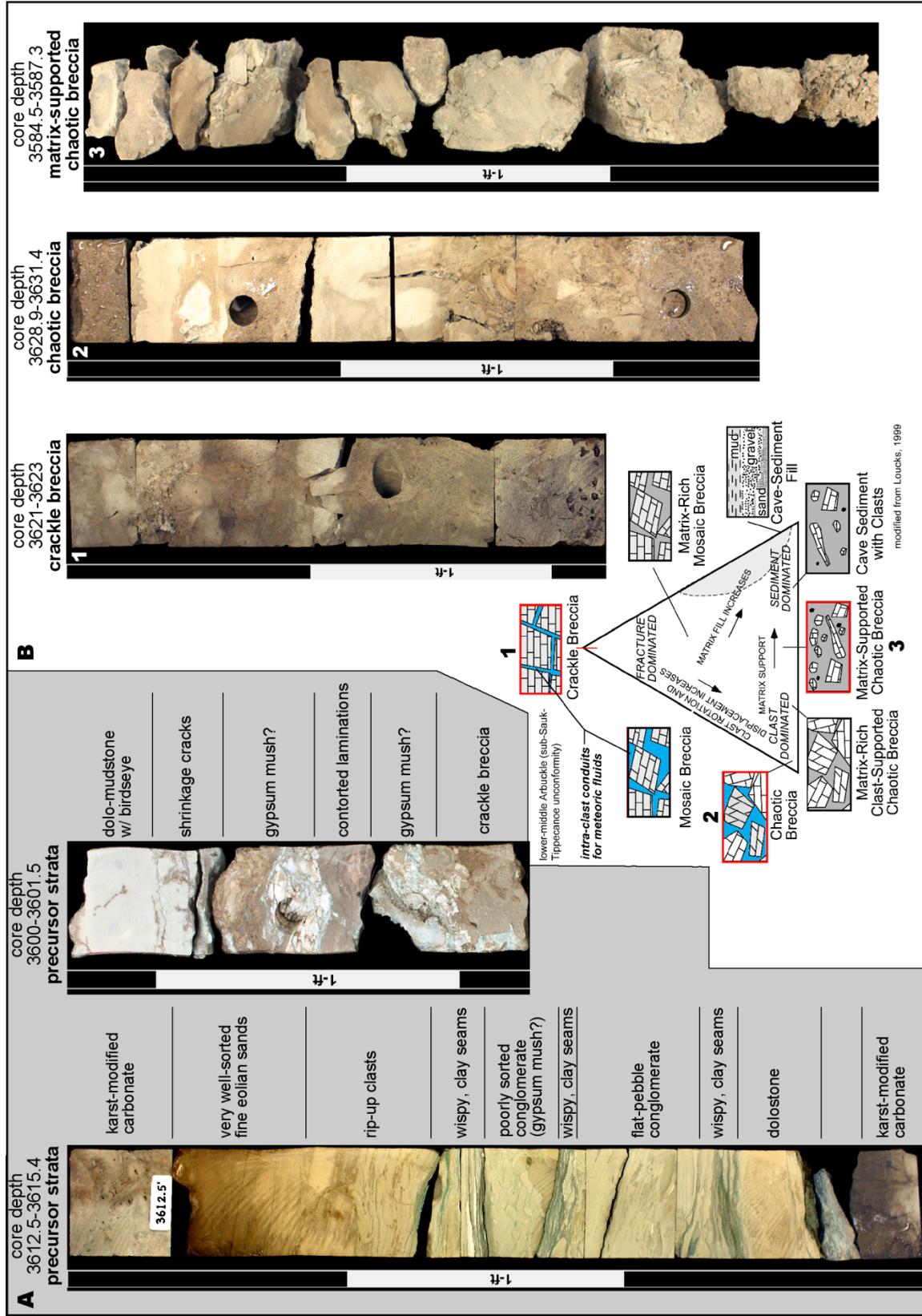
Figure 4. Facies common in the L. Hadley-4 core. Observations from image logs (McCord-A 20H) and core suggest two distinct karst phases. This includes syndepositional evaporite karst and post-Arbuckle vadose karst (Early Ordovician–pre-Mississippian). See text for further discussion.

11
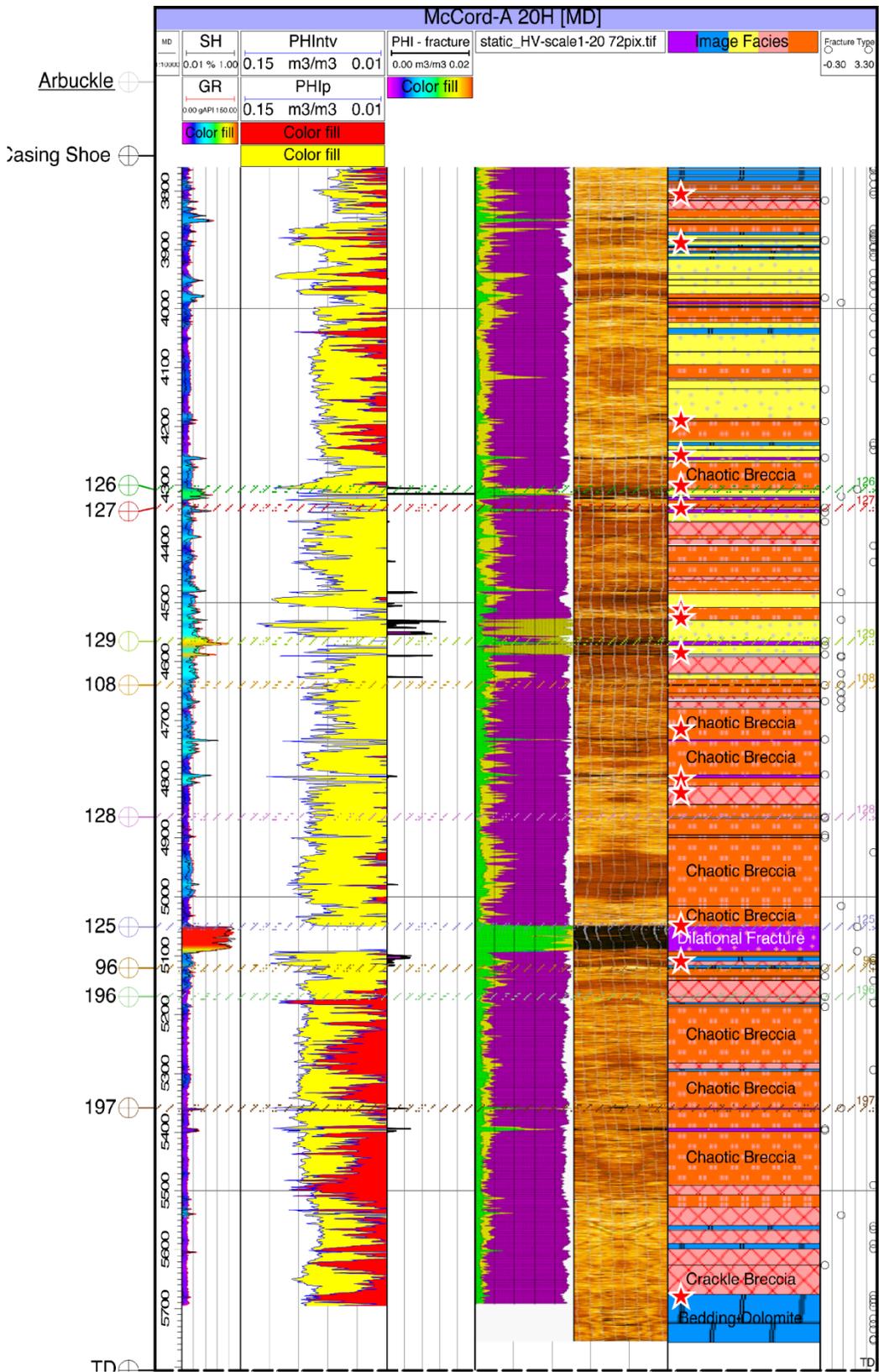
Figure 5. McCord-A 20H image log interpretation. Red stars indicate facies examples shown in Figures 6–14.
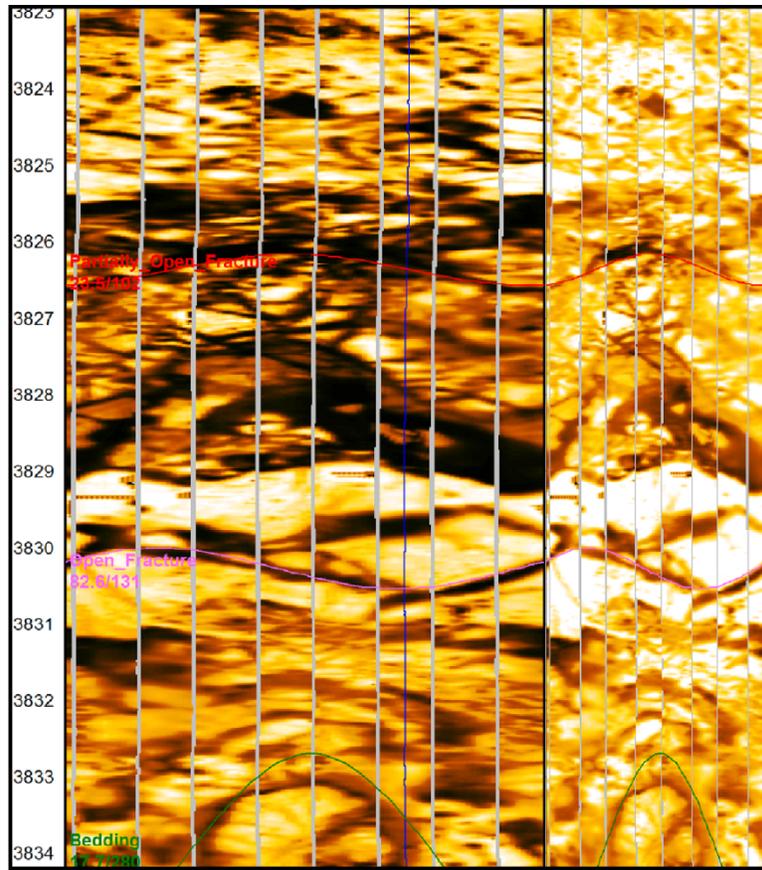
Crackle Breccia
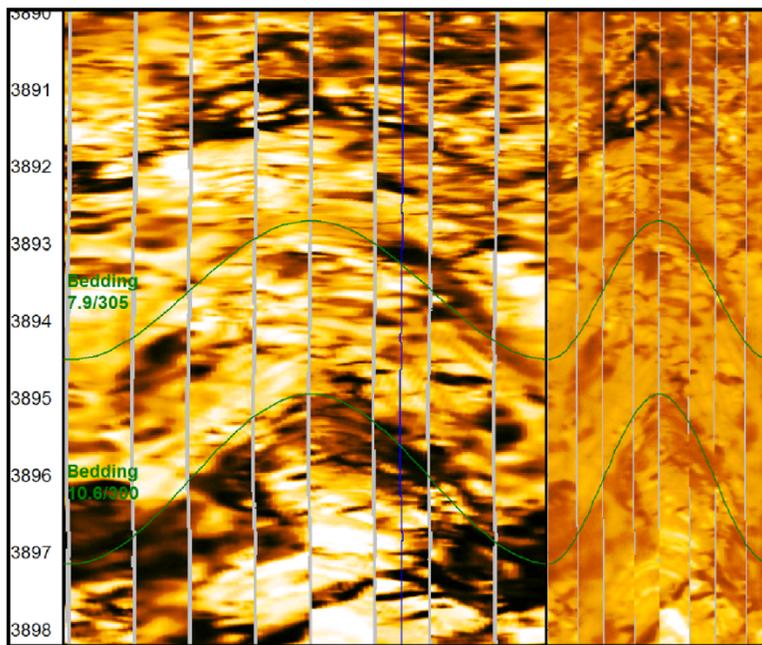
Beddding

Figure 6. McCord-A 20H image log examples.
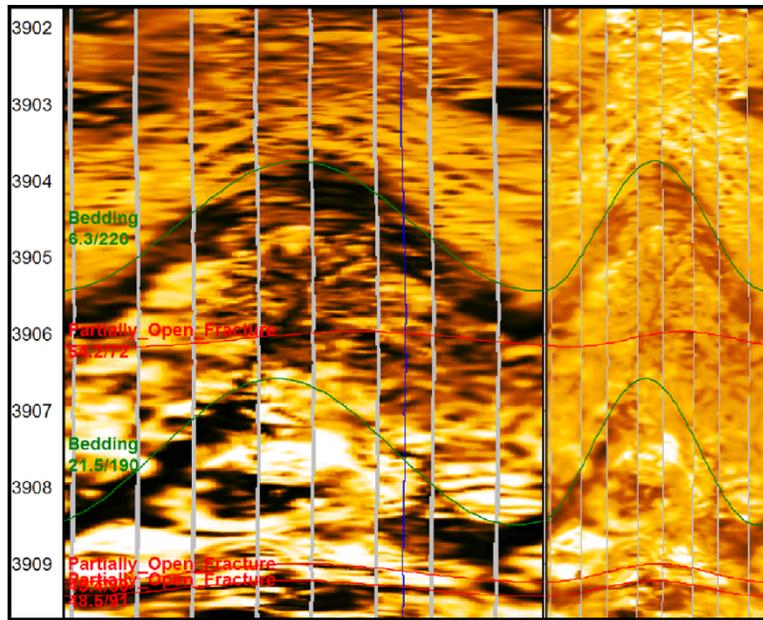
Beddding
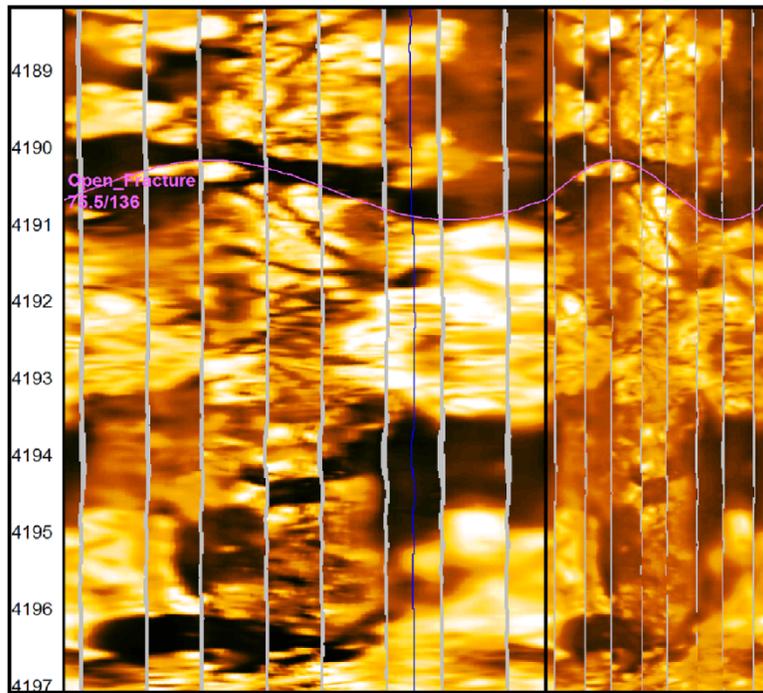
Open Fracture

Figure 7. McCord-A 20H image log examples.

Open Fracture


Matrix-Supported Breccia
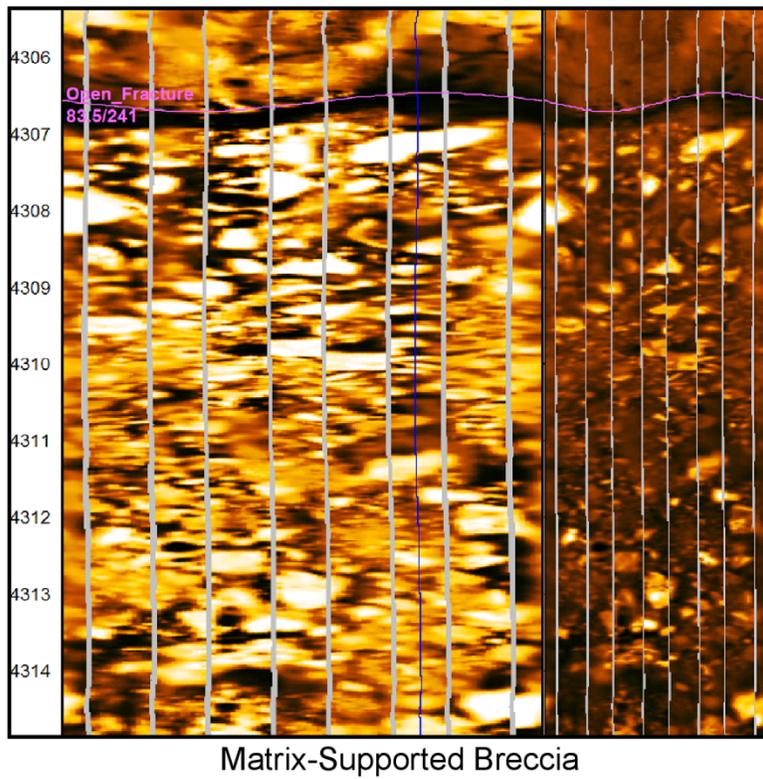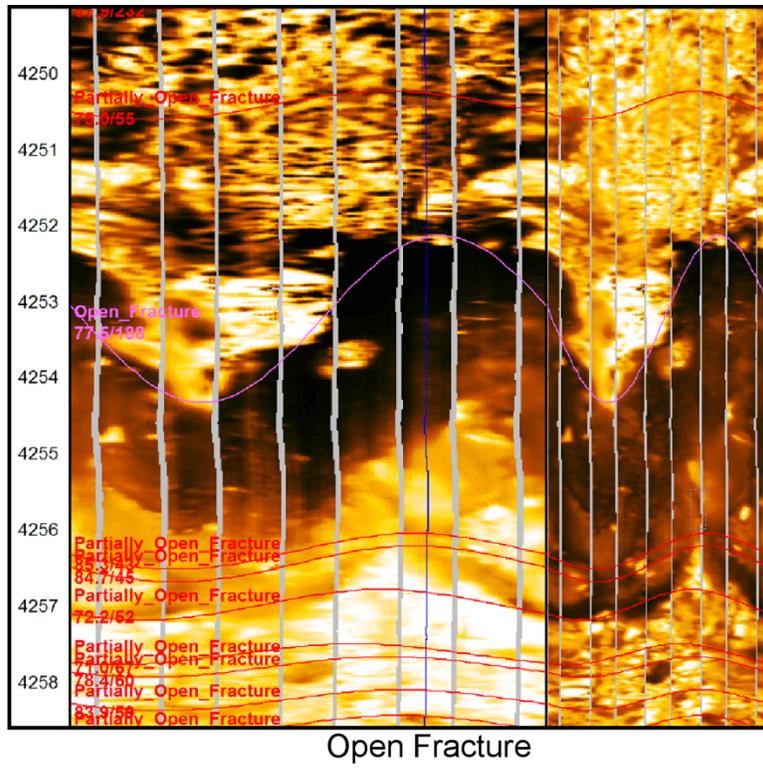
Figure 8. McCord-A 20H image log examples.
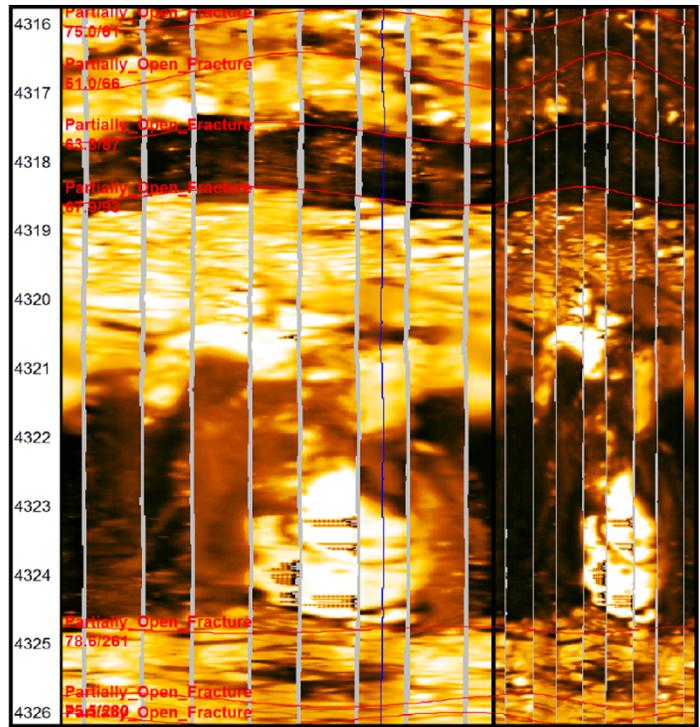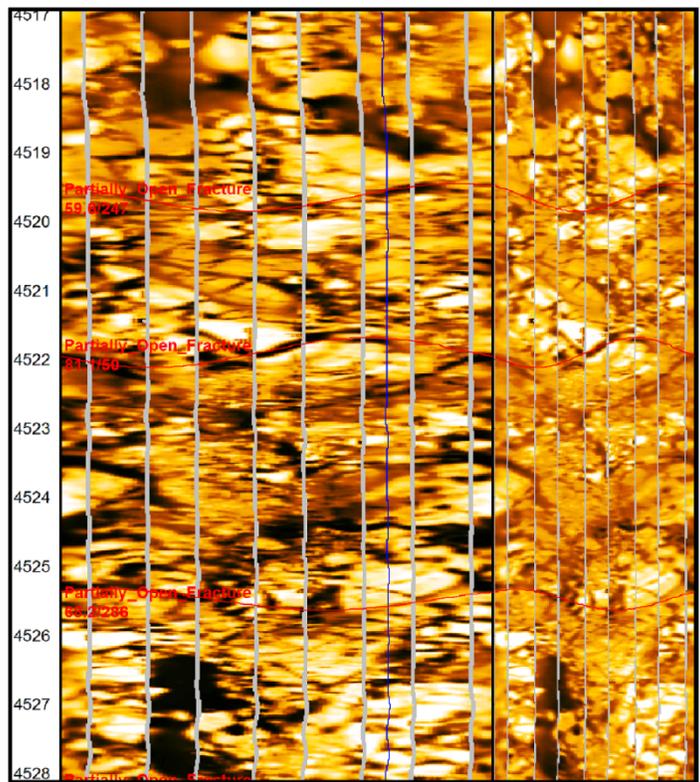
Open Fracture

Chaotic Breccia

Figure 9. McCord-A 20H image log examples.

Figure 10. McCord-A 20H image log examples.
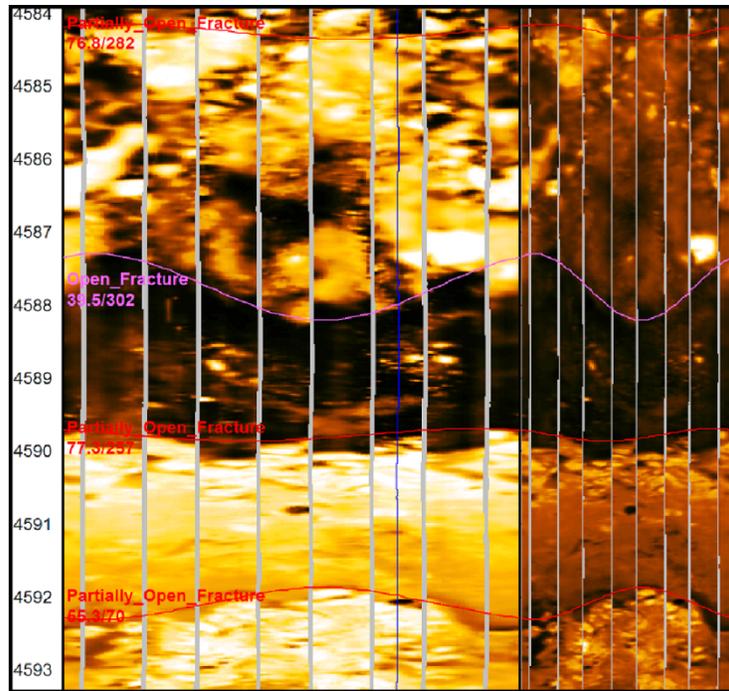
Open Fracture
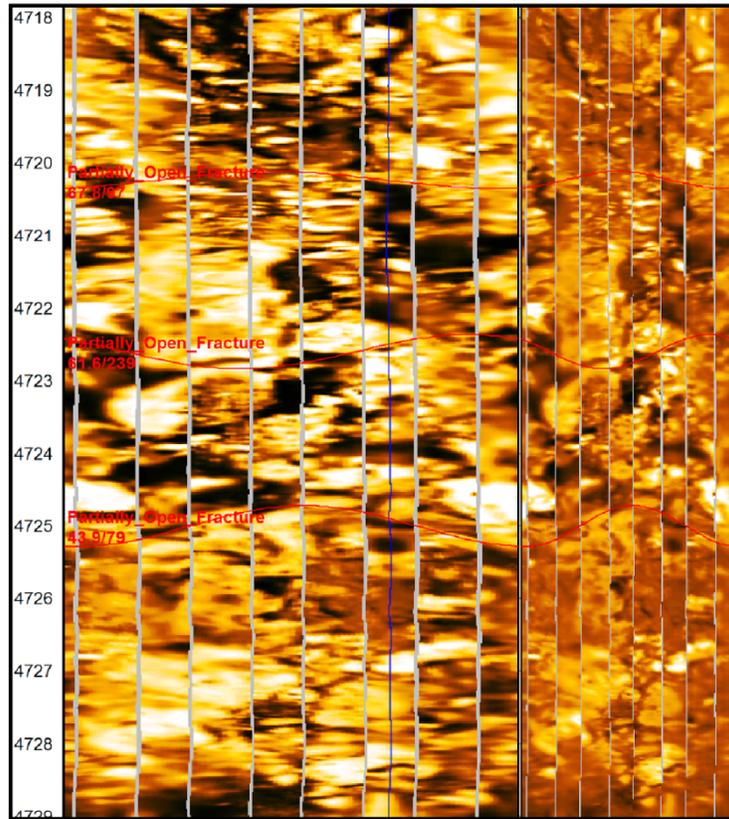
Chaotic Breccia

Figure 11. McCord-A 20H image log examples.
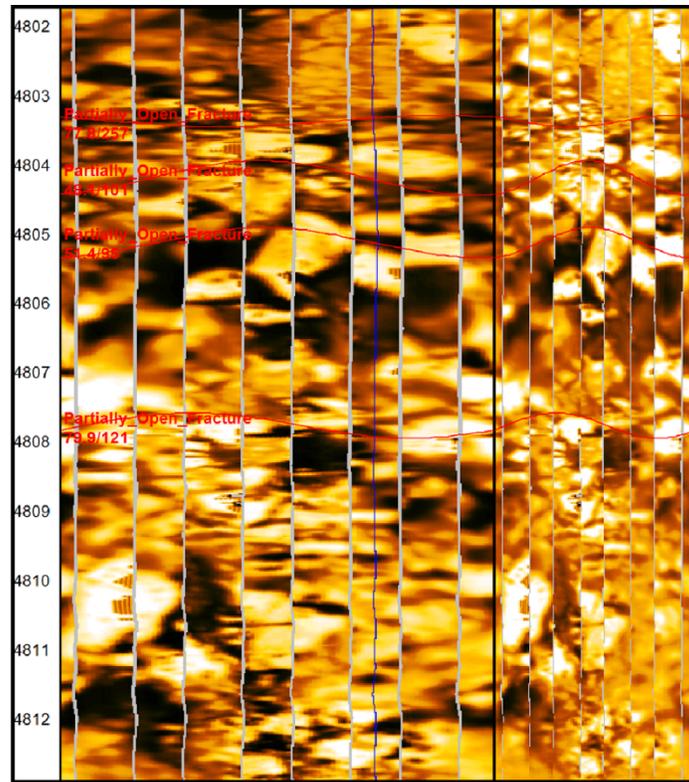
Chaotic Breccia
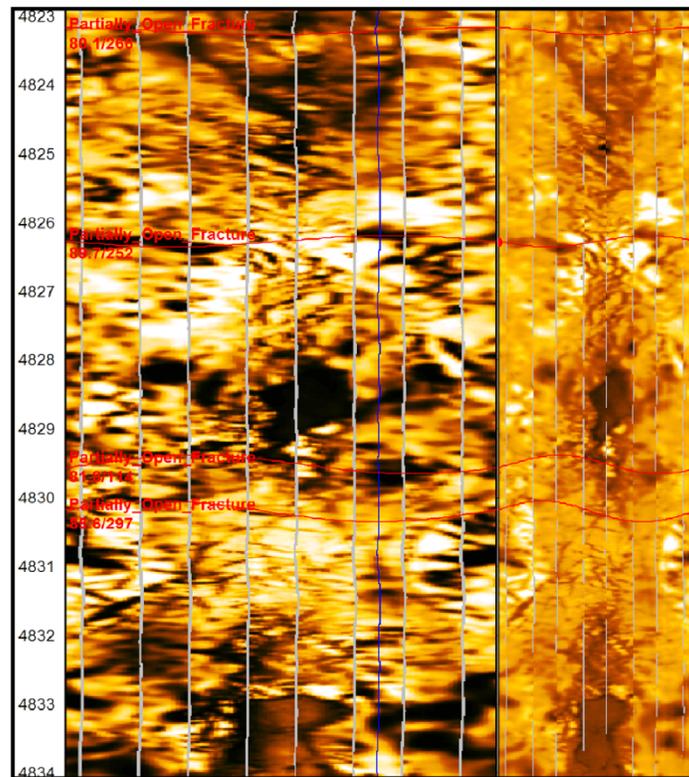

Crackle Breccia

Figure 12. McCord-A 20H image log examples.
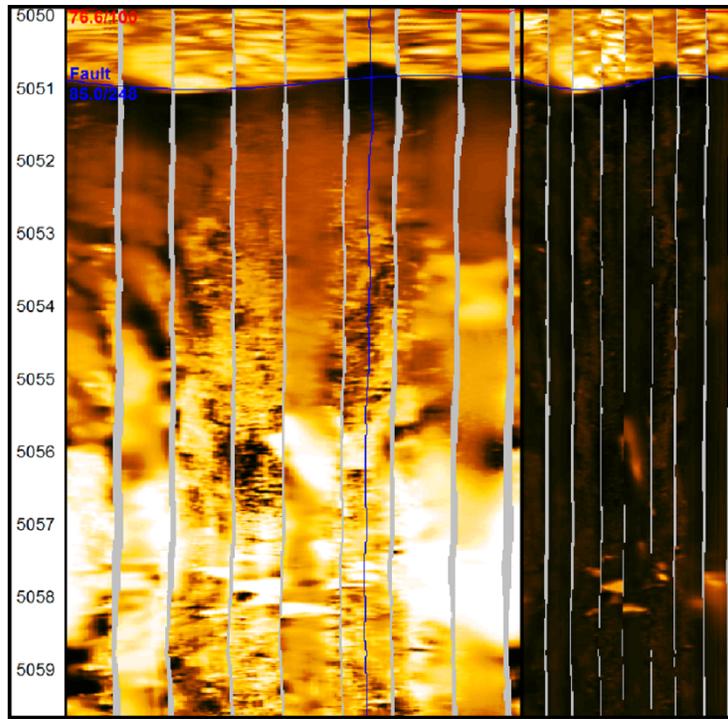
Fault
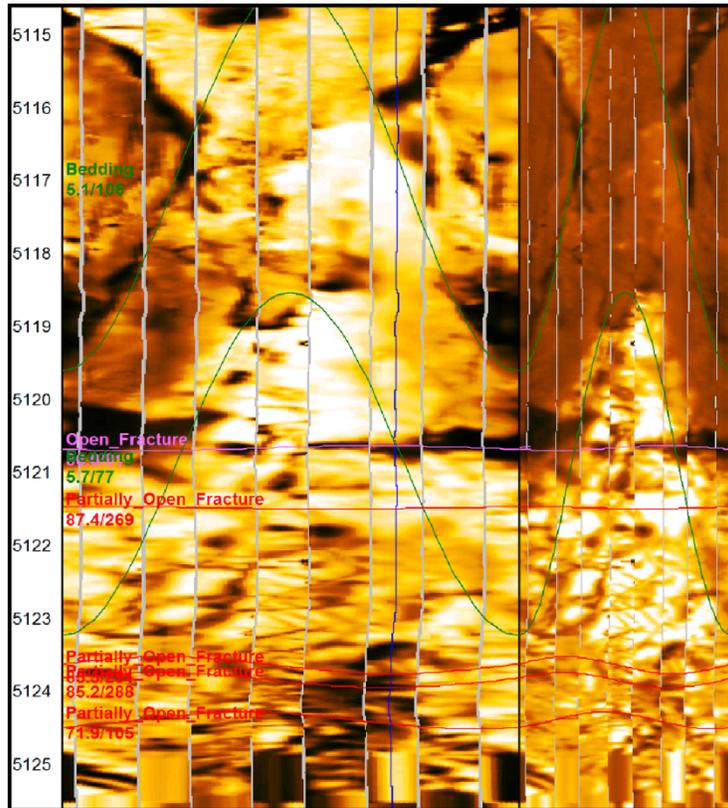
Crackle Breccia

Figure 13. McCord-A 20H image log examples.
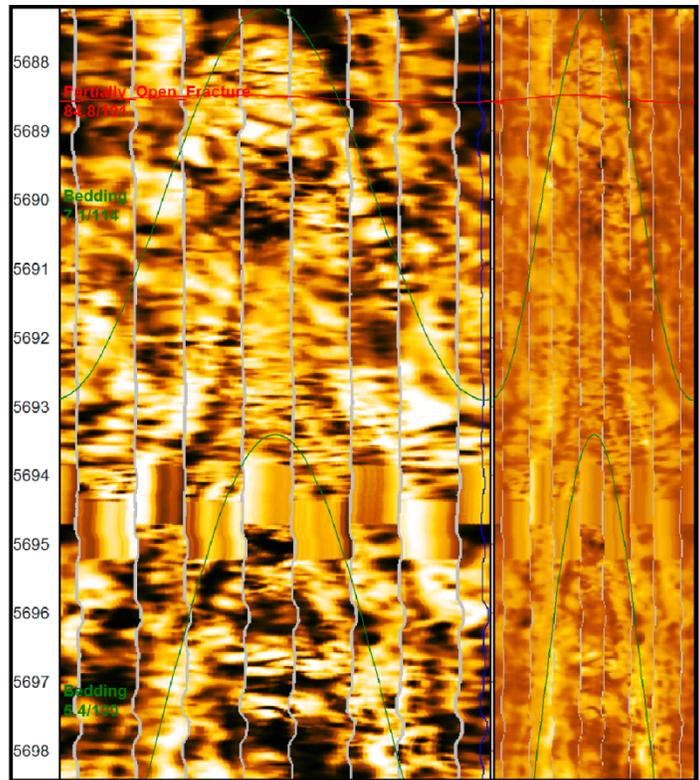
Bedding/Moldic
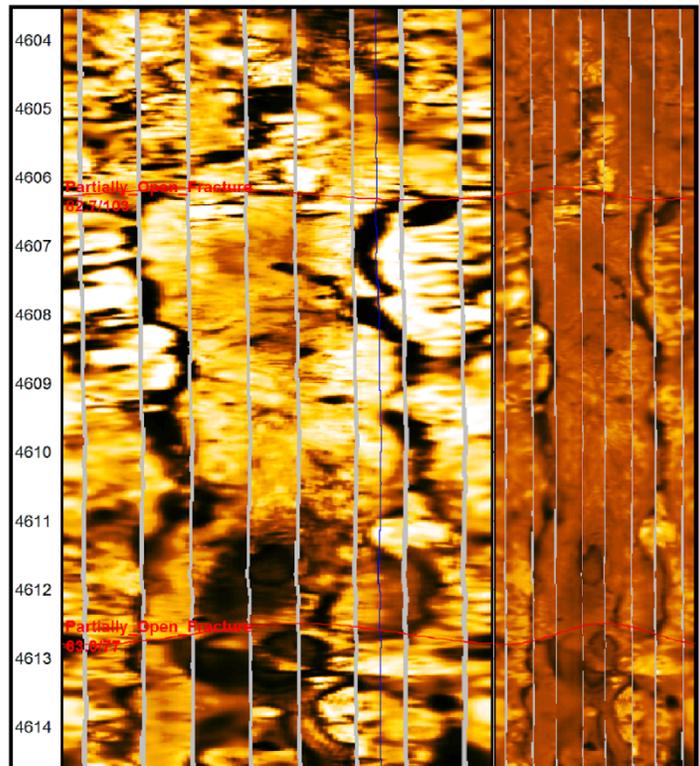
Borehole Breakout (Induced fractures)

Figure 14. McCord-A 20H image log examples.
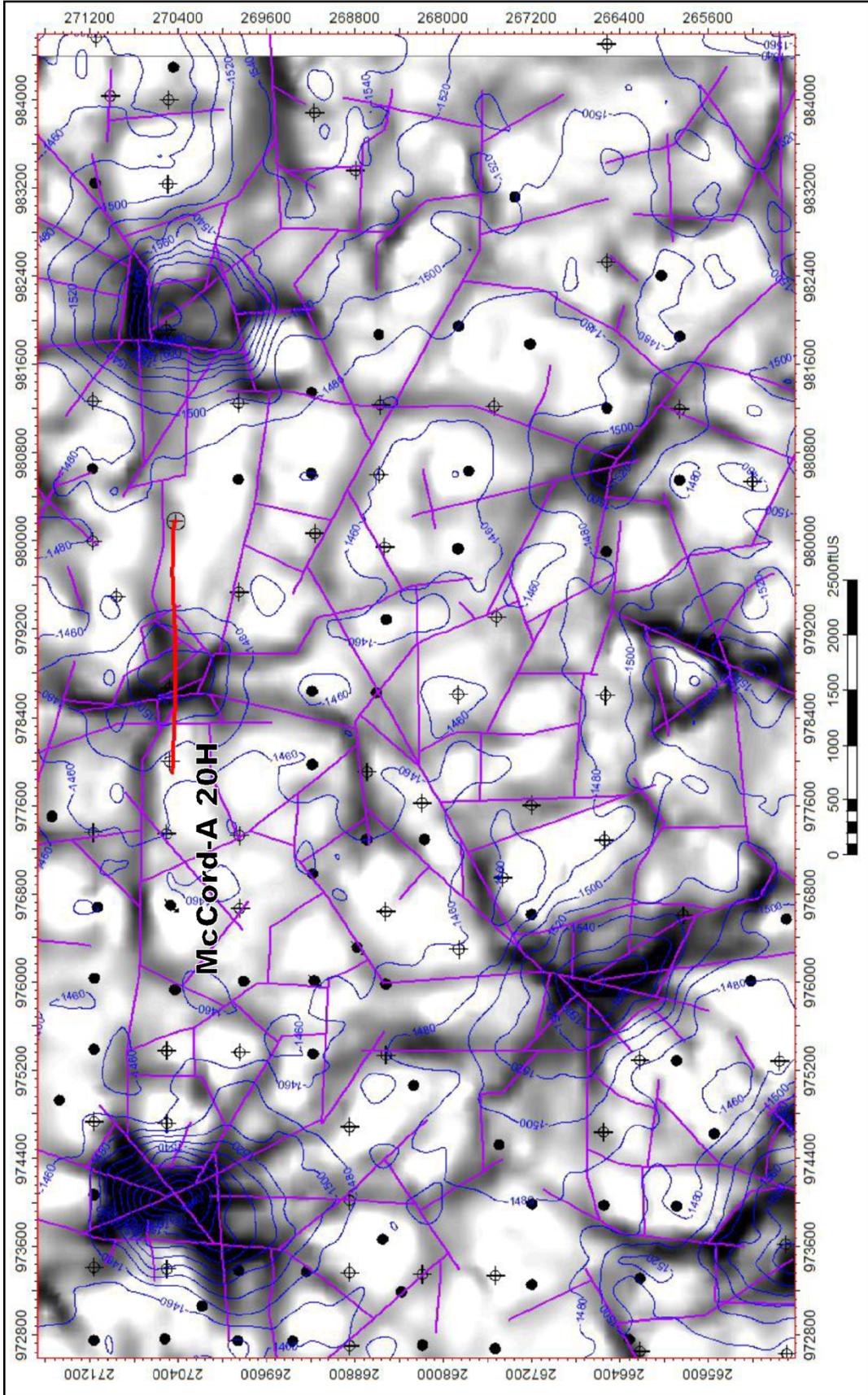
Figure 15. Map showing distribution volumetric curvature attribute and fault model for simulation study area.
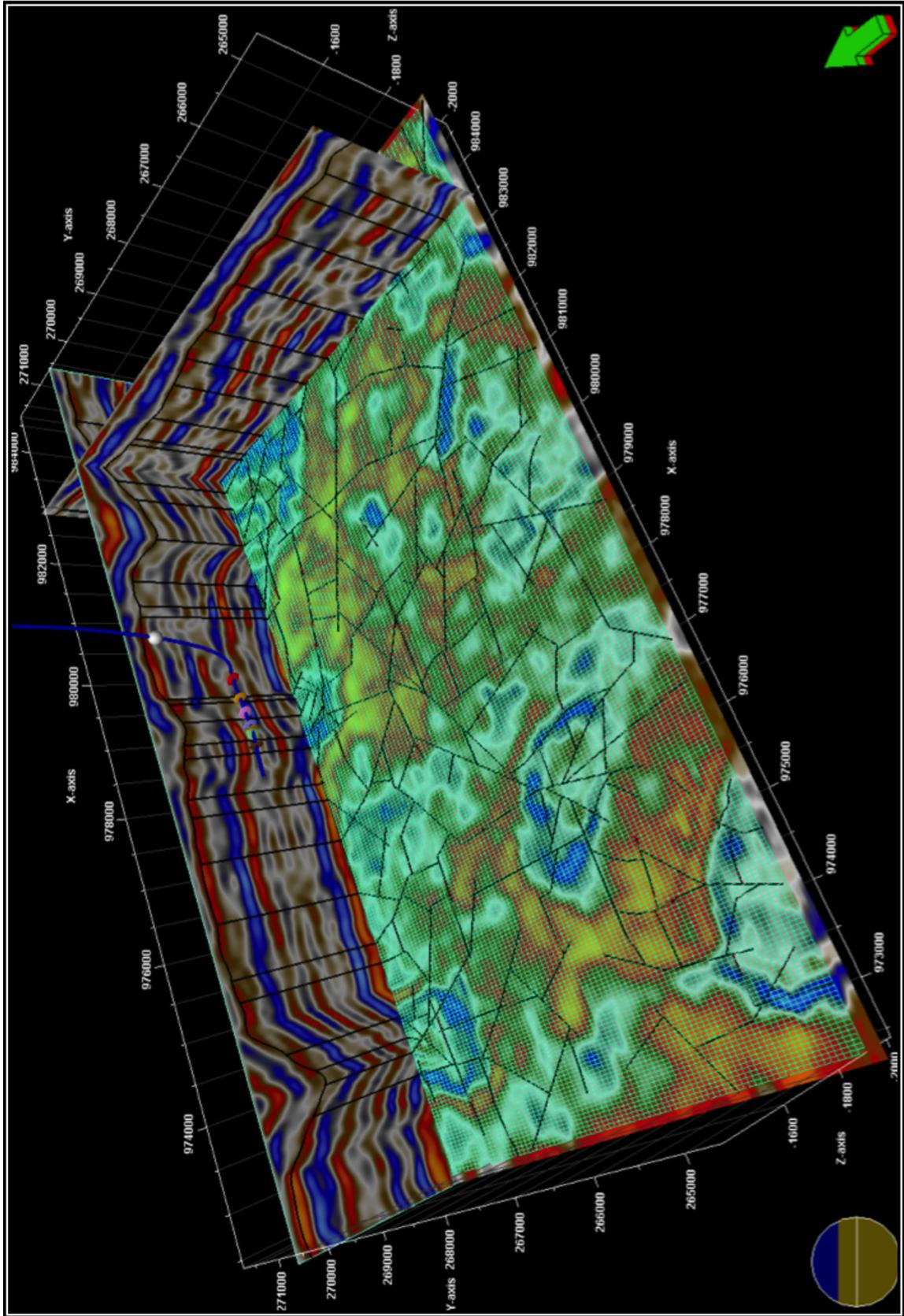
Figure 16. 3-D model showing seismic, fault intersections, simulation grid, and the McCord-A 20H with fault and fracture picks interpreted from image log. The fault model, derived from the VC map, correlates well with the major fault sets observed in the 3-D PSDM seismic volume.

23
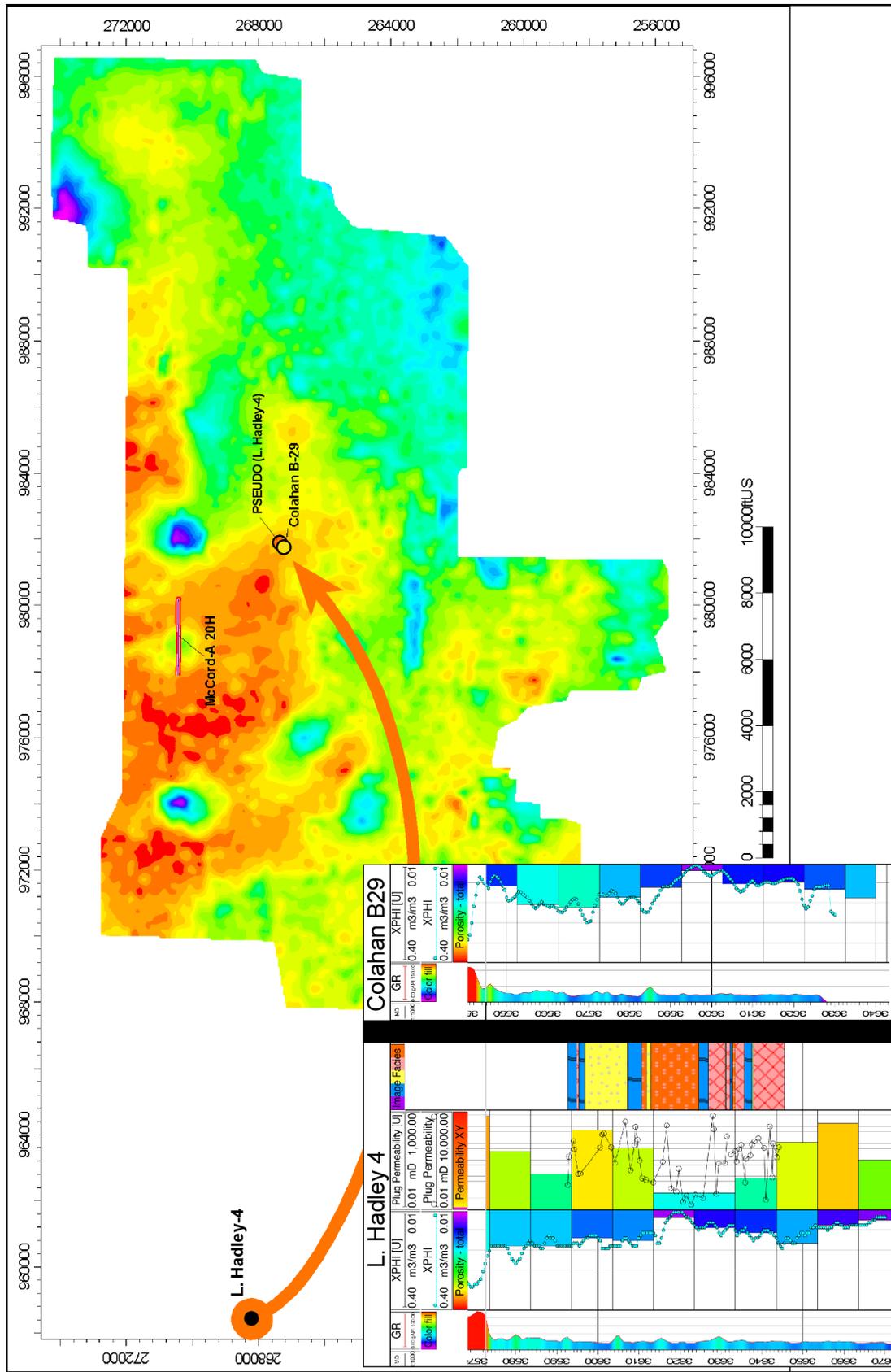
Figure 17. Map showing location of nearest Arbuckle well (L. Hadley-4) with core and permeability data. Cores recovered from the L. Hadley-4 reveal similar breccia fabrics as those observed from the McCord-A 20H. Colahan B-29 gamma ray and porosity logs are most consistent with logs from the L. Hadley-4. Because of these similarities, the L. Hadley-4 was used as a pseudo well to provide facies and permeability data for modeling algorithms.
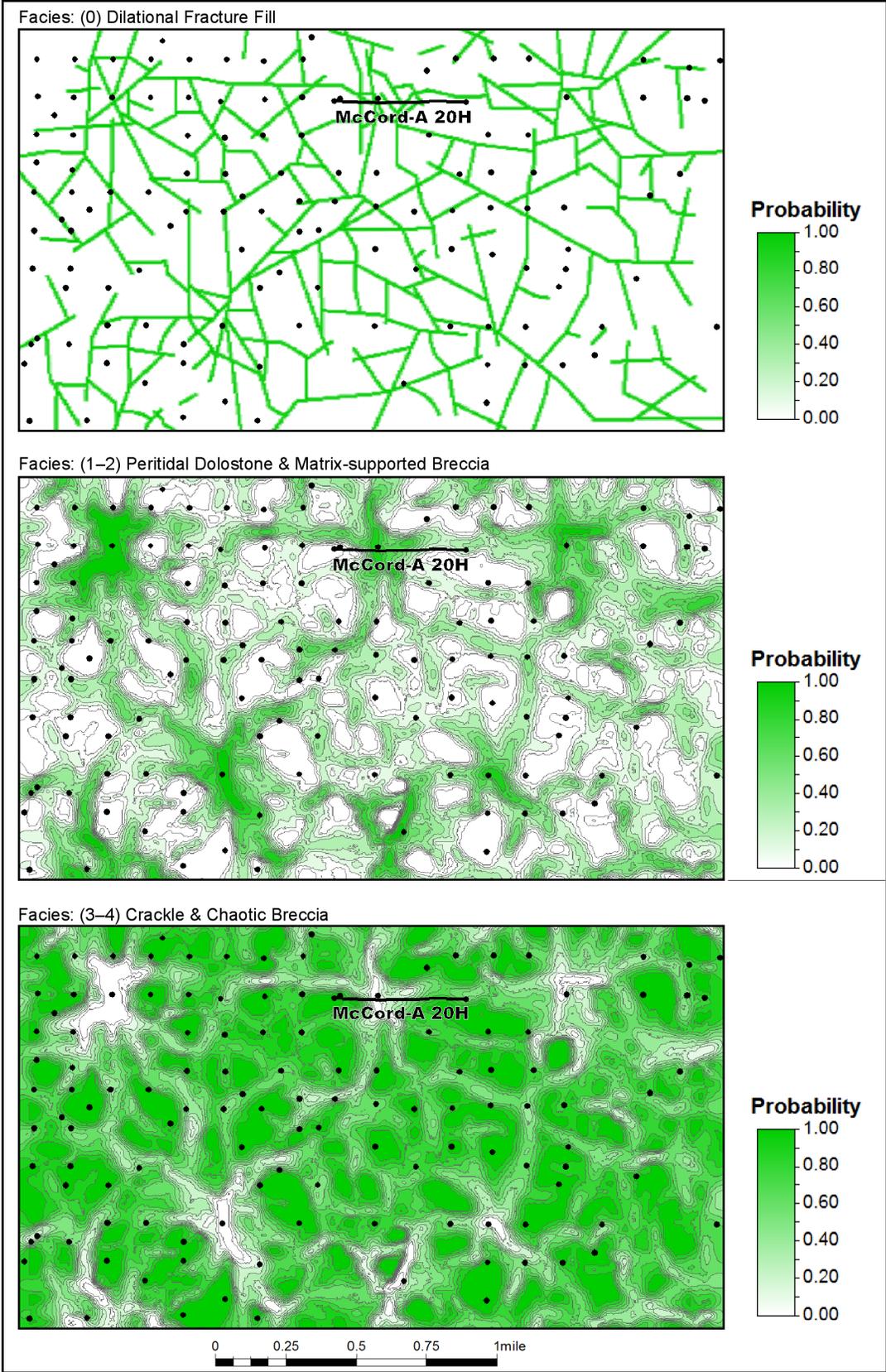
Figure 18. Probability maps used for conditioning facies and petrophysical models.
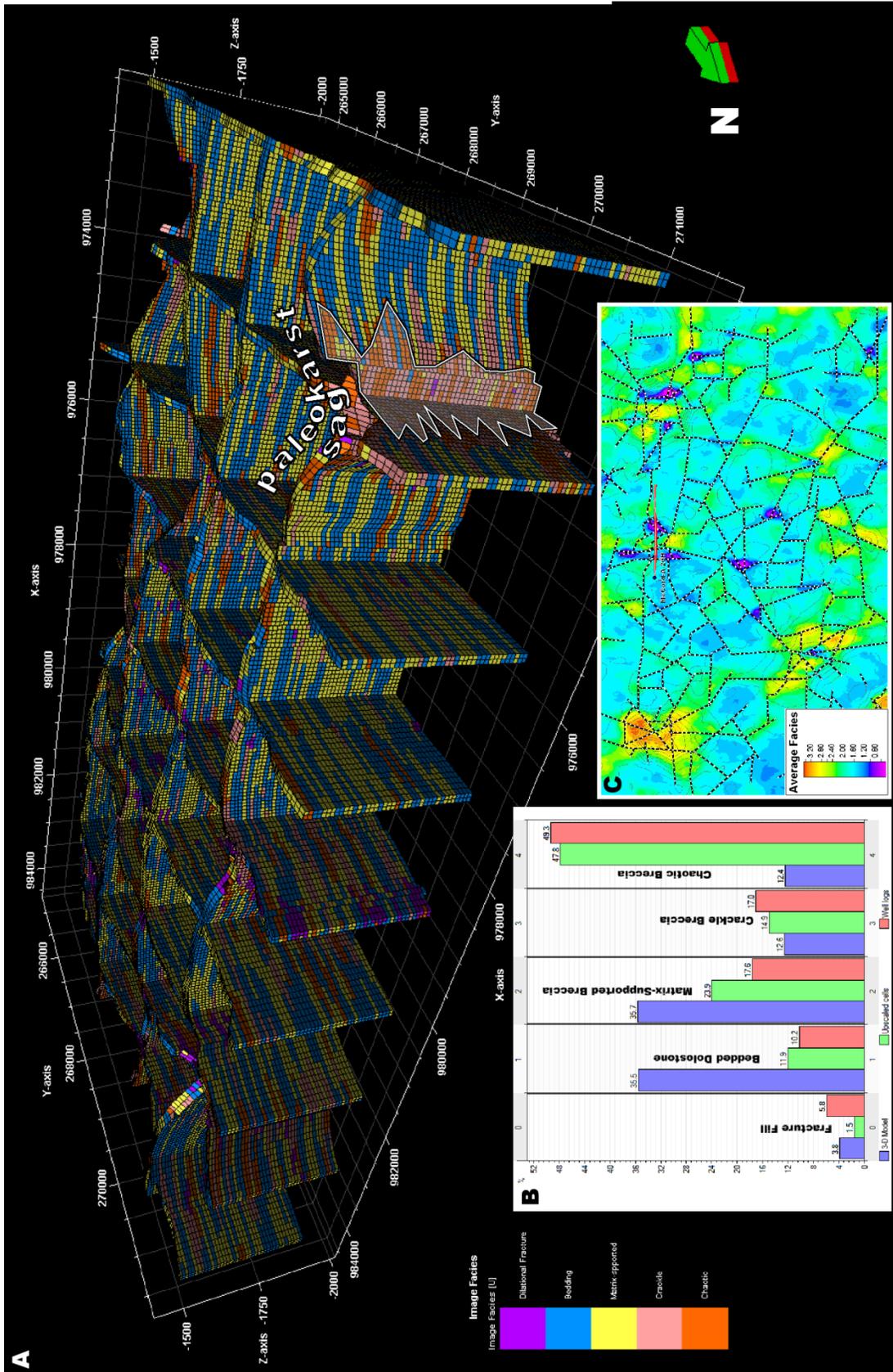
Figure 19. A) Three-dimensional fence diagram showing facies model. Notice how crackle and chaotic breccias are concentrated within paleokarst sags whereas bedded dolomites and matrix-supported breccias populate host strata. This model was constructed using sequential indicator simulation and facies trend maps. **B)** Histogram showing facies distribution for logs, upscaled logs, and 3-D model. **C)** Map showing facies distribution after vertically averaging the entire 3-D porosity model. This map reveals a facies distribution consistent with paleokarst trends.
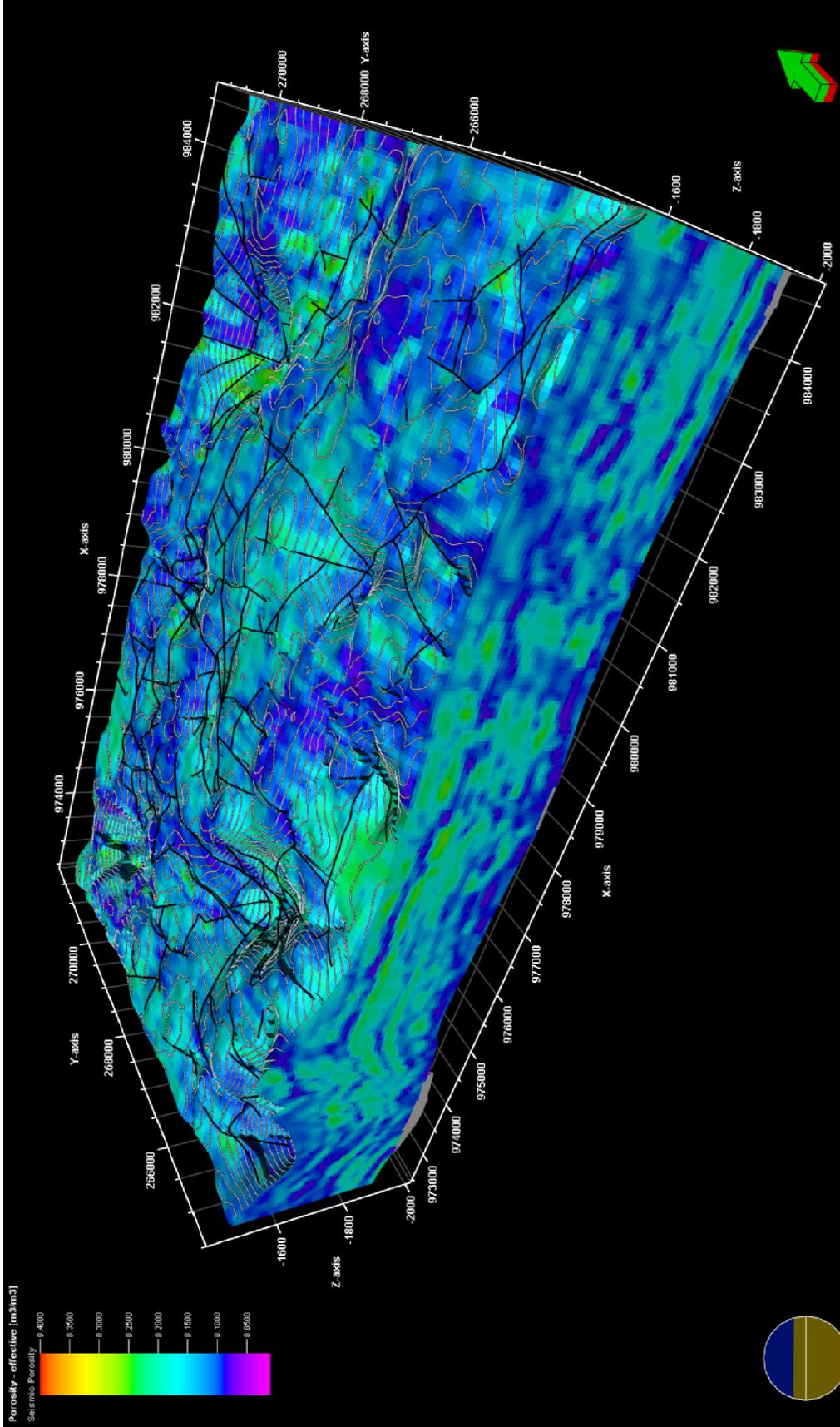
Figure 20. Three-dimensional grid of the PSDM seismic porosity attribute volume that was generated using genetic seismic inversion.
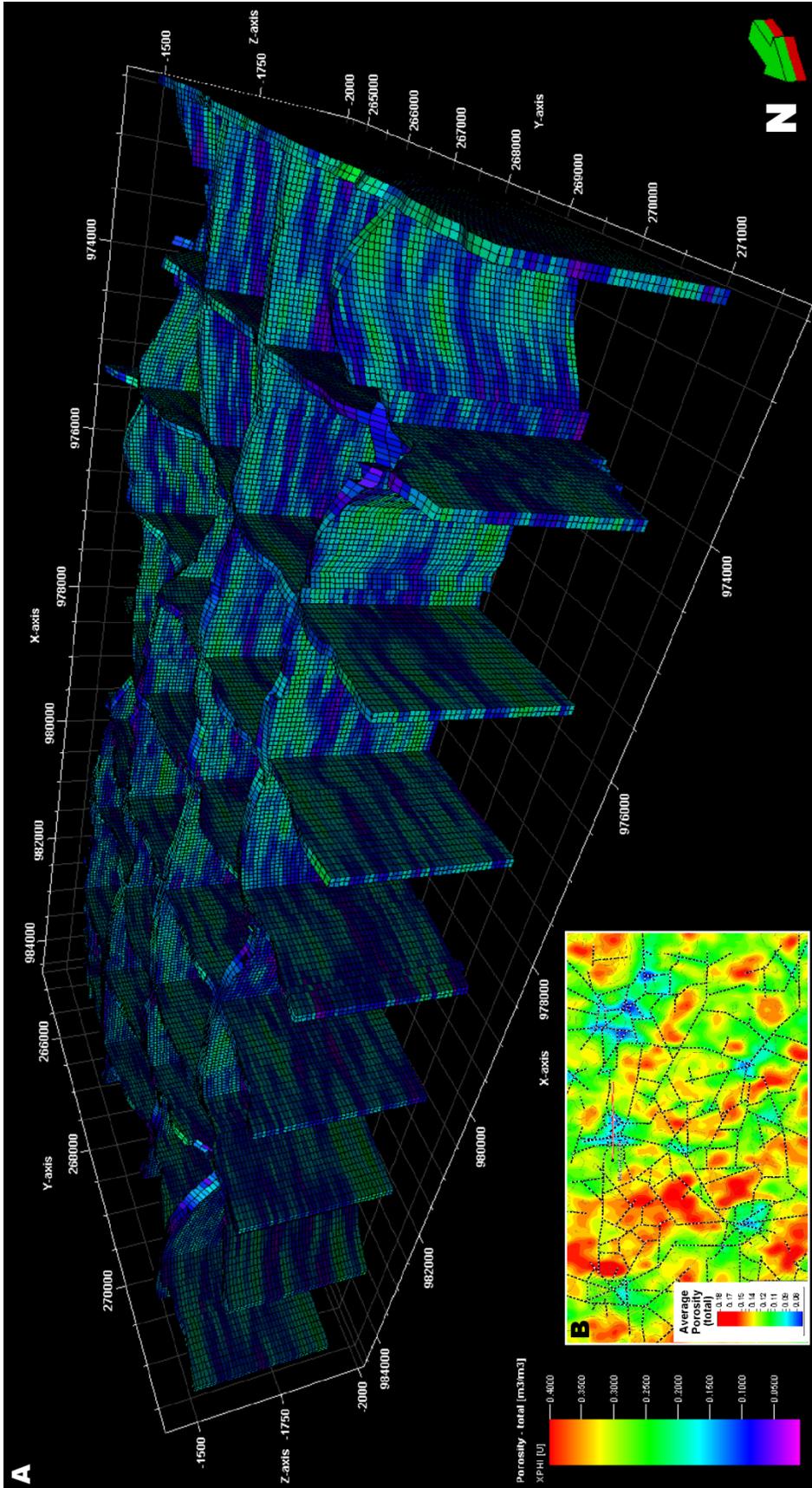
Figure 21. A) Three-dimensional (3-D) fence diagram showing final porosity model. The model was generated using upscaled total porosity logs biased to the facies model. The modeling method was sequential Gaussian simulation using normal distributions per facies, trend maps, and collocated co-Kriging (where secondary variable = seismic porosity grid). **B)** Map showing porosity distribution after vertically averaging the entire 3-D porosity model. This map reveals prosity distribution consistent with the McCord-A 20H.
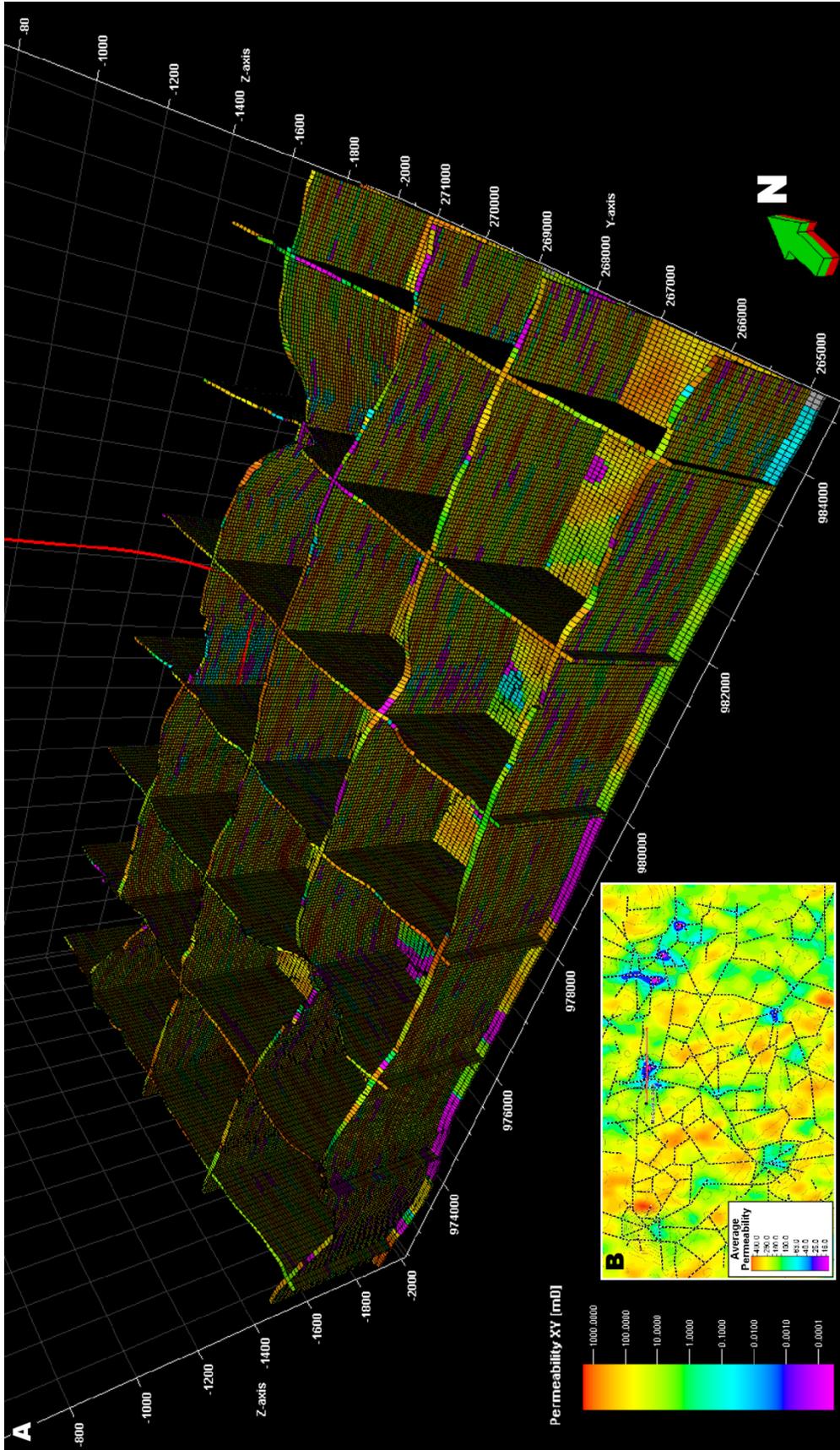
Figure 22. A) Three-dimensional (3-D) fence diagram showing permeability model. The model was generated using upscaled permeability logs biased to the facies model. The modeling method was sequential Gaussian simulation using log normal distributions per facies, trend maps, and collocated co-Kriging (where secondary variable = porosity model). **B)** Map showing permeability distribution after vertically averaging the entire 3-D permeability model. This map reveals a permeability distribution consistent with the McCord-A 20H low porosity observed within the paleocavern.

29
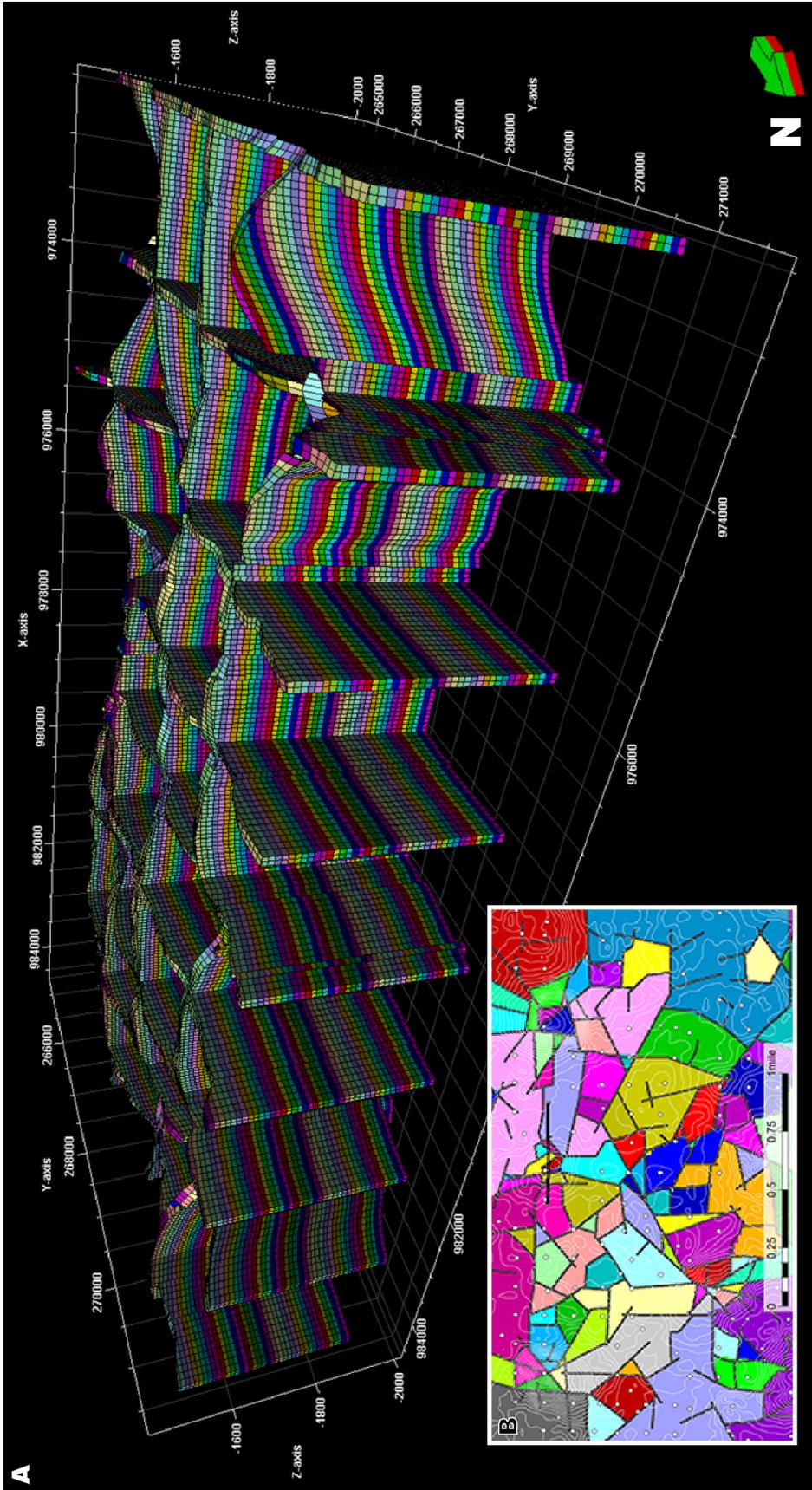
Figure 23. A) Three-dimensional image showing layering used in models. Conformable layering was constructed from bottom to top. Notice truncated layers across top surface that is consistent with post-Arbuckle erosional and karst processes. **B)** Map showing fault-bound segments. Each segment can be simulated as a block or as multi-block sectors with different fluxes across faults.
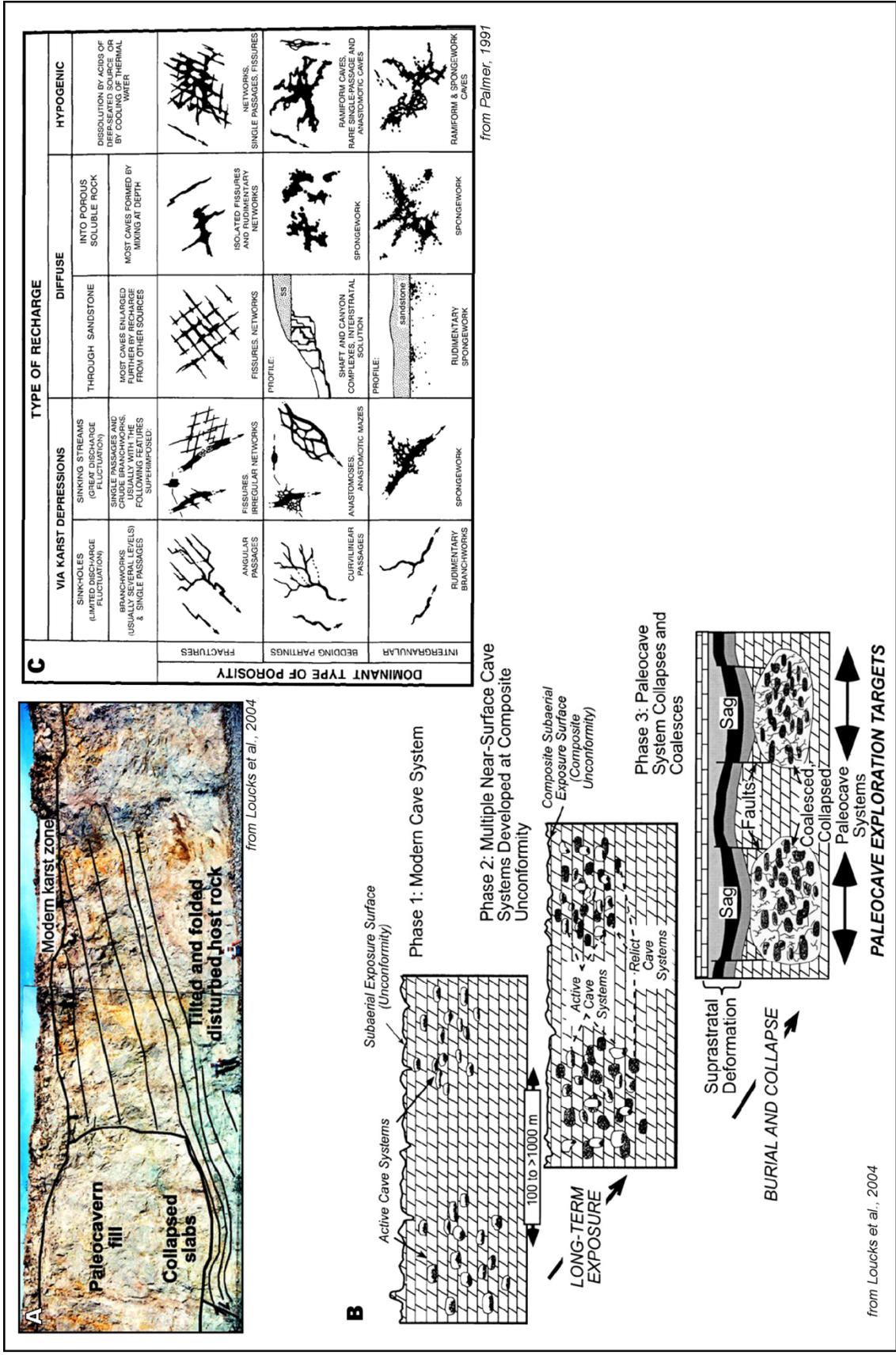
Figure 24. A) Photo showing horizontal juxtaposition of paleocavern and a collapsed strataform, cave ceiling (figure from Loucks et al., 2004). **B)** Schematic diagram developmental stages of a collapse paleocave (figure from Loucks et al., 2004). **C)** Typical cave patterns and their relationships to recharge and cavernous porosity (figure from Palmer, 1991).

REFERENCES

Loucks, R.G., 1999, Paleocave carbonate reservoirs; origins, burial-depth modifications, spatial complexity, and reservoir implications: AAPG Bulletin, v. 83, p. 1795-1834.

Loucks, R.G., Mescher, P.K., and McMechan, G.A., 2004, Three-dimensional architecture of a coalesced, collapsed-paleocave system in the Lower Ordovician Ellenburger Group, central Texas: AAPG Bulletin, v. 88, p. 545-564.

Kerans, C., 1988, Karst-controlled reservoir heterogeneity in Ellenburger Group carbonates of West Texas: AAPG Bulletin, v. 72, p. 1160-1183.

Palmer, A.N., 1991, Origin and morphology of limestone caves: Geological Society of America Bulletin, v. 103, p. 1-21.

Attachment 1   COST PLAN/STATUS - NOTE ALL BPs UPDATED WITH REVISED SF-424A SUBMITTED FOR BP2 CONTINATION APPLICATION EFF 1/1/12

PREPARED BEFORE DOE CHANGED BP2 TO START 4/30/12, RATHER THAN 1/1/12

	BP1 Starts: 10/1/10 Ends: 4/29/12					BP2 Starts: 4/30/12 Ends: 4/29/13			
Baseline Reporting Quarter	10/1/10-12/31/10 Q1	1/1/11 - 3/31/11 Q2	4/1/11 - 6/30/11 Q3	7/1/11 - 9/30/11 Q4	10/1/11 - 12/31/11 Q5	1/1/12 - 3/31/12 Q6	4/1/12 - 6/30/12 Q7	7/1/12 - 9/30/12 Q8	10/1/12 - 12/31/12 Q9
Baseline Cost Plan (from SF-424A)	(from 424A, Sec. D)								
Federal Share	$332,669.00	$332,668.00	$332,668.00	$332,668.00	$0.00	$48,318.50	$48,318.50	$48,318.50	$48,318.50
Non-Federal Share	$82,826.75	$82,826.75	$82,826.75	$82,826.75	$0.00	$11,306.75	$11,306.75	$11,306.75	$11,306.75
Total Planned (Federal and Non-Federal)	$415,495.75	$415,494.75	$415,494.75	$415,494.75	$0.00	$59,625.25	$59,625.25	$59,625.25	$59,625.25
Cumulative Baseline Cost	$415,495.75	$830,990.50	$1,246,485.25	$1,661,980.00	$1,661,980.00	$1,721,605.25	$1,781,230.50	$1,840,855.75	$1,900,481.00
Actual Incurred Costs	thru 12/31/10	thru 3/31/11	thru 6/30/11	thru 9/30/11	thru 12/31/11	thru 3/31/12	thru 6/30/12	thru 9/30/12	thru 12/31/12
Federal Share	$16,716.32	$83,793.01	$33,922.88	$36,036.00	$5,452.27	$700,073.33	$299,938.01	$82,751.96	$43,586.41
Non-Federal Share	$3,044.15	$10,391.64	$9,721.74	$5,023.69	$2,609.95	$678.59	$0.00	$327,172.60	$5,233.09
Total Incurred Costs-Quarterly (Federal and Non-Federal)	$19,760.47	$94,184.65	$43,644.62	$41,059.69	$8,062.22	$700,751.92	$299,938.01	$409,924.56	$48,819.50
Cumulative Incurred Costs	$19,760.47	$113,945.12	$157,589.74	$198,649.43	$206,711.65	$907,463.57	$1,207,401.58	$1,617,326.14	$1,666,145.64
Variance									
Federal Share	$315,952.68	$248,874.99	$298,745.12	$296,632.00	-$5,452.27	-$651,754.83	-$251,619.51	-$34,433.46	$4,732.09
Non-Federal Share	$79,782.60	$72,435.11	$73,105.01	$77,803.06	-$2,609.95	$10,628.16	$11,306.75	-$315,865.85	$6,073.66
Total Variance-Quarterly (Federal and Non-Federal)	$395,735.28	$321,310.10	$371,850.13	$374,435.06	-$8,062.22	-$641,126.67	-$240,312.76	-$350,299.31	$10,805.75
Cumulative Variance	$395,735.28	$717,045.38	$1,088,895.51	$1,463,330.57	$1,455,268.35	$814,141.68	$573,828.92	$223,529.61	$234,335.36

Attachment 2: Schedule/Milestone Status

Milestone	Task/Subtask	Project Milestone Description	Project Duration - Start: Jan 1, 2010 End: Dec 31, 2013													Planned Start Date	Planned End Date	Actual Start Date	Actual End Date	Comments (notes, explanation of deviation from plan)
			Project Year 1					Project Year 2				Project Year 3								
			Q1	Q2	Q3	Q4	Q5	Q6	Q7	Q8	Q9	Q10	Q11	Q12	Q13					
1.1	2.1	Obtain 3D seismic, grav/mag, remote sensing, logs														10/1/10	1/1/11	10/1/10	1/31/01	Delay in data confidentiality negotiations and tracing missing logs
1.2	2.2–3.9	Complete initial pre-spud geomodel														10/1/10	3/31/11	2/10/11	9/30/11	PSDM & VC volumes delivered. VC interpretation in progress. BP1 extension granted
1.3	4.1–4.3	History match and forecast.														3/1/11	6/13/11	9/30/11		Will complete early BP2
1.4	5.1–6.8	Drill, Log, and Test Bore-hole #1 (McCord A 20H)														5/1/11	7/31/11	8/12/11	11/24/11	Bore-hole and horizontal lateral successfully drilled and logged.
2.1	7.1–7.5	Complete Formation Evaluation														7/31/11	12/31/11	11/24/11	12/31/11	Final formation evaluation and seismic attribute interpretations will be correlated
2.2	8.1–8.4	Complete VC and inversion														1/1/12	6/30/12	1/1/12	7/30/12	Complete final VC interpretation and seismic inversion
2.3	9.1–9.5	Complete structural and facies models														9/31/12	12/31/12	9/31/12	12/31/12	Completed.